

https://dspace.org/

Modelling of gas recovery from unconventional reservoir shale gas

Khari, Andile

2019

https://hdl.handle.net/10539/28838

Khari, Andile Aubrey (2019) Modelling of gas recovery from unconventional reservoir shale gas, University of the Witwatersrand, Johannesburg, <http://hdl.handle.net/10539/28838>

Downloaded from a DSpace repository. https://dspace.org/



Modelling of Gas Recovery from Unconventional Reservoir Shale Gas.

Master of Sciences by coursework and research
(MSc 50/50)

Prepared by

Student name: Mr. Andile Khari

Student number: 0710368P

Submitted to

School of Chemical and Metallurgical Engineering, Faculty of Engineering and the Built Environment, University of the Witwatersrand, Johannesburg, South Africa

Supervisor(s): Dr Ezekiel Madigoe & Dr Diakanua Nkazi

Date: 04 February 2019

ABSTRACT

It is believed that petroleum gas is stored as free gas in natural fractures, free gas in pores, adsorbed gas and dissolved gas in kerogen bulk in the shale. Hydraulic Fracking is used to promote free gas flow to production well, but adsorbed and dissolved gas is not recovered and usually ignored. This work looks into modifying existing gas flow model, by including mechanisms that can promote and contribute to shale gas production recovery during reservoir depletion. The developed model includes non-Darcy flow which is suitable for high-velocity gas flow. Model equation was simulated with the help of MATLAB to solve the partial derivative equation to achieve a shale gas production a 3D profile of pressure vs time vs distance. The model results were seen behaving similarly to available developed models, whereby pressure is initially increasing and then decrease overtime. The initial increase in pressure is due to the free gas available in natural fractures and micro-fracture in the matrix and is produced first causing pressure to increase. During production, overtime free gas in these natural fractures and micro-fracture gets depleted, causing pressure to decrease and approach critical desorption pressure over time. The free gas in the matrix nanopores feed these depleted fracture networks, the kerogen nanopores is in turn fed by adsorbed and dissolved gas on kerogen inside the nanopores surface which take place at later stage of production. The developed model shows similar gas recovery production behaviour with the laboratory results, which proves that the proposed model can be used to predict the production profile.

ACKNOWLEDGEMENTS

First and foremost, I would like to thank my supervisor Dr Diakanua Nkazi for his guidance and advice from the day I started my Master's degree, up until today. I am truly grateful for his support and assistance when I needed help the most.

I would also like to thank my Msc colleagues for the support we have given each other throughout the course.

Special thanks to my family for encouraging words, love and support since the day I started school.

Finally, I would like to thank Batong Mamabolo and Mike Dlulane for their help with MATLAB software. I am truly grateful.

Table of Contents

ABSTRACT ..... **ii**
ACKNOWLEDGEMENTS ..... **iii**
LIST OF FIGURES ..... **vi**
LIST OF TABLES ..... **viii**
NOMENCLATURE ..... **ix**
CHAPTER 1: INTRODUCTION **1**
1.1 Background **1**
1.2 Problem Statement **4**
1.3 Research Aim and Objectives **4**
1.3.1 Aim 4
1.3.2 Objectives 5
CHAPTER 2: LITERATURE REVIEW **6**
2.1 Shale Gas Exploration **6**
2.2 Horizontal well with Multistage Fracturing Technique **7**
2.3 Shale gas flow **11**
2.4 Pore space **14**
2.4.1 Pores within Organic Matter 14
2.4.2 Pores within Matrix 15
2.4.3 Pore space characterisation 16
2.5 Diffusion **19**
2.6 Adsorption/desorption **23**
2.7 Langmuir and BET Isotherm **28**
CHAPTER 3: GAS RECOVERY MODEL DEVELOPMENT **32**
3.1 Continuity equation for shale gas **32**
3.1.1 Conservation of Mass 33
3.1.2 non-Darcy effect 38
3.1.3 Klinkenberg effect 38
3.1.4 Sink/Source term 39
3.1.5 Adsorption 41
3.1.6 Diffusion effect 41
CHAPTER 4: SIMULATION RESULTS AND DISCUSSION **43**

CHAPTER 5: CONCLUSION AND FUTURE WORK 52
Conclusion 52
Future work 53
REFERENCES 55
APPENDIX A 57
APPENDIX B 60

LIST OF FIGURES

Figure 1.1 World natural production by type (Energy Infromation Administration, 2016) 2

Figure 1.2 Natural gas production by type in China, Canada, and the United State (Cao, 2017) .. 3

Figure 2.1 Main Karoo basin showing the location of the cores studied (Adams, 2016)..... 7

Figure 2.2 Gas production in shale gas reservoirs within different scales (Cao, 2017) 8

Figure 2.3 Illustration of gas flow from nanoscale to macroscale (Zhang, Xu, & Jiang, 2017)..... 9

Figure 2.4 Gas injection schematic in horizontal well with multi-hydraulic fractures (Wan, 2013) 10

Figure 2.5 Well production schematic in horizontal well with multi-hydraulic fractures (Wan, 2013) 10

Figure 2.6 Gas distribution in shale strata from macro-scale to micro-scale showing free gas in fractures, free gas and adsorbed gas in the matrix (Guo, 2015). 12

Figure 2.7 Gas flow behaviour in the matrix during production (Li, 2016). 13

Figure 2.8 Variation in nanopores morphology in organic matter (Guo, 2015)..... 15

Figure 2.8 3D representation of single cell (Berawala, 2015) 17

Figure 2.8 Gas flow mechanism in a nano pore. Red represents Knudsen diffusion, and blue represents viscous flow (Guo, 2015) 18

Figure 2.9 Pore diameter change due to methane gas desorption; (a) adsorbed and free gases inside a nanopore, (b) increased pore diameter due to desorption (Swami, 2013)..... 18

Figure 2.10 (a) Darcian flow due to pressure gradient; (b) Darcian flow due to pressure gradient and Fickian flow due to the concentration gradient (Yu et al., 2016). 19

Figure 2.11 Types of gas diffusion in Shale (Chen et al., 2018) 21

Figure 2.12 Relationship between the shale gas diffusion capacity and pore diameter (Chen et al., 2018) 21

Figure 2.13 Free, adsorbed and total gas content (scf/rcf) vs pressure for Barnet Shale (Mengal, 2010) 24

Figure 2.14 Fraction of adsorbed gas, free gas to total vs pressure for Barnet Shale (Mengal, 2010) 25

Figure 2.15 Marcellus Shale adsorption gas content (Berawala, 2015) 25

Figure 2.16 Schematic plot of monolayer and multilayer gas adsorption; (a) Monolayer Langmuir adsorption, (b) Multilayer BET adsorption (Yu et al., 2016)..... 31

Figure 4.1 Developed model simulation in 3D showing pressure vs time vs distance..... 44

Figure 4.2 Developed model simulation in 2D showing pressure vs time 44

Figure 4.3 Gas evolution and production for shale sample (Javadpour et al., 2007)..... 46

Figure 4.4 Dissociation of experimental data into four flow regimes ; fractures, matrix (nanopores), desorption and diffusion from kerogen bulk (Swami, 2013)..... 47

Figure 4.5 Comparison of various storage and transport mechanisms. Also validation with experimental work (Swami, 2013)..... 48

Figure 4.6 Simulation results for cumulative gas recovery after 40 days (Swami, 2013)..... 48

Figure 4.7 Gas recovery behaivoir..... 50

LIST OF TABLES

Table 1. Experimental data of the first injection test (Prusty Harpalani, S., 2004). 27

Table 2. Experimental data of the second injection test (Prusty Harpalani, S., 2004). 28

NOMENCLATURE

Symbols

$\boldsymbol{V_s}$	volume of a phere
B_g	gas formation volume factor
Z	compressibility factor
V_c	volume of cube
ρ_{gsc}	gas density at standard condition
S_g	Gas saturation
P_L	Langmuir reservoir pressure
$\emptyset m$	porosity of the matrix
Pi	initial reservoir pressure
Ci, m	concentration within the matrix
Dm	Diffusion coefficient in the matrix
δ	dimensionless constrictivity factor
V_b	bulk volume
ρ_R	density of shale at initial reservoir pressure
V_L	maximum amount of adsorbed gas
P_{ad}	equilibrium pressure
p_0	saturation pressure of the gas
v_m	maximum adsorption gas volume

k	permeability
μ	fluid viscosity
ρ_g	fluid density
$\emptyset$	porosity
c_f	pore volume compressibility
c_t	total compressibility
c	fluid compressibility
D_{k}	Knudsen diffusion coefficient
∇p	pressure gradient
β	Forchheimer parameter
K_n	Knudsen number

Abbreviations

CBM	Coal-bed methane
TOC	total organic carbon
CCS	carbon capture and storage
BET Isotherm	Branauer Emmet Teller Isotherm
EGR	Enhanced Gas Recovery
EOR	Enhanced Oil Recovery
SEM	Scanning Electron Microscope

CHAPTER 1: INTRODUCTION

1.1 Background

Shale gas has become an increasingly important source of natural gas due to the depletion of oil reservoirs and global environmental problems which see the use of natural gas as the cleanest source of energy compared to fossil fuels (Li, 2016). Shale rock consists of shale gas in organic-rich formations that are both source rock and reservoir. These reservoirs are known as unconventional due to the ultra-low permeability and porosity of shale rock, trapping the source methane within them. These shale properties make it difficult to use the conventional vertical well drilling technique to extract gas which produces insufficient gas and therefore becomes uneconomical. However, over the past decade, the application of two techniques; horizontal drilling and hydraulic fracturing has made it possible to extract gas economically from shale formations (Li, 2016). The United States is the leading and very advanced country in the exploration of Shale gas using these two techniques. Barnett Shale geological formation near Fort Worth, Texas in the US, used these techniques to produce gas, which demonstrated that they could be key to producing trillions of cubic feet of natural gas estimated (Li, 2016). Furthermore, Argentina, Canada and China are other countries that have commercial shale gas production. The more technological developments advance in the future, the more health and safety issues are understood. It is expected that this will encourage the extraction of shale gas in other countries.

Natural gas production over the world is projected to rise from 342 billion cubic feet per day in 2015 to 554 Bcf/d by 2040 (EIA, 2016). The largest proportion of this growth is shale gas production, which increases from 42 Bcf/d to 168 Bcf/d by 2040 shown in Figure 1.1 Furthermore, shale gas is expected to account for 30% of world natural gas production by the end of the forecast period. The rise of natural gas use is due to countries moving to cleaner fuels to mitigate global warming. The United States shale gas production accounted for more than half of U.S natural gas production in 2015 according to production stats published by U.S Energy Information Administration. These stats showed how much shale gas exploration and production activities are taking place in the US. China has drilled more than 600 shale gas wells and

produced 0.5 Bcf/d of shale gas as of 2015.Furthermore, Shale gas is projected to account for more than 40% of the country's total natural gas production by 2040, which would make China the second largest shale gas producer in the world after the U.S as seen in Figure 1.2 (Energy Infromation Administration, 2016). Major shale gas reserves are known to exist in about 46 countries, and over 50% of the reserves are in China, Argentina, Algeria, United States and Canada. South Africa is one of the countries that has discovered shale gas in the Karoo Basin and has shown interest in exploring and producing it. The developments have not been started yet, due to environmental concerns caused by the hydraulic fracking process.

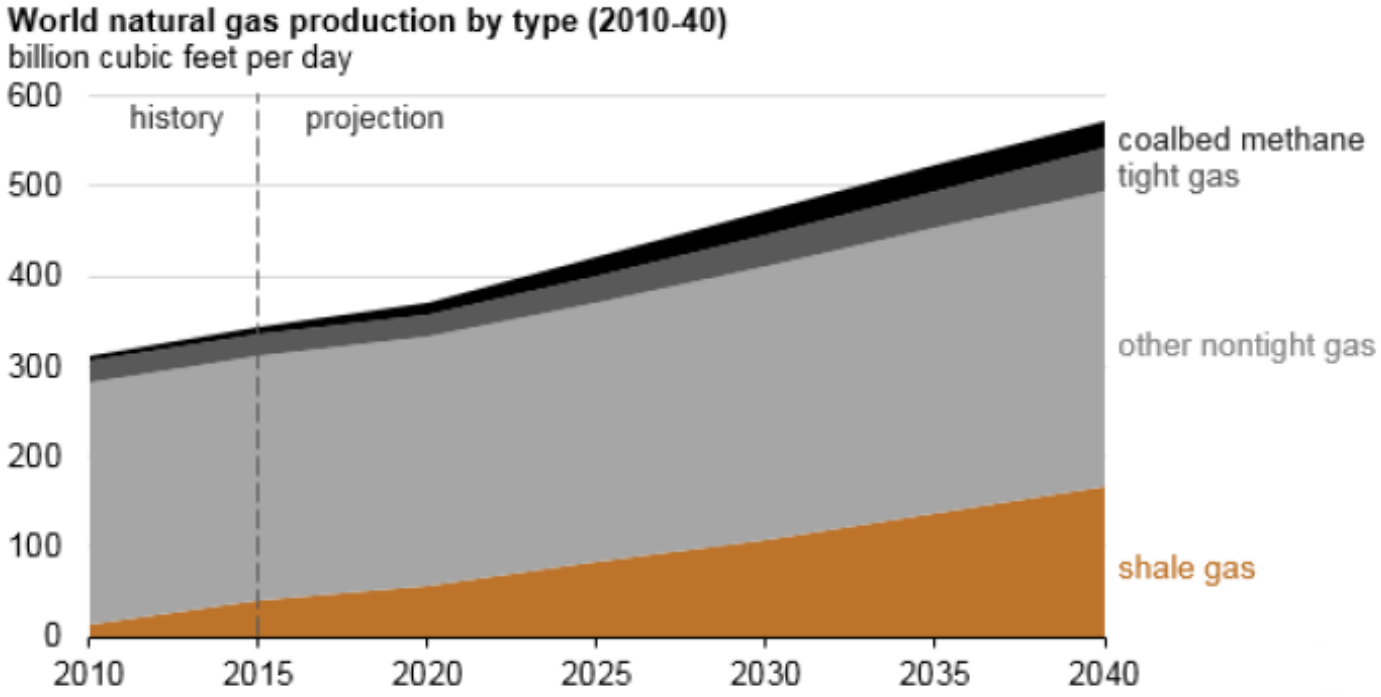


Figure 1.1 World natural gas production by type (Energy Infromation Administration, 2016)

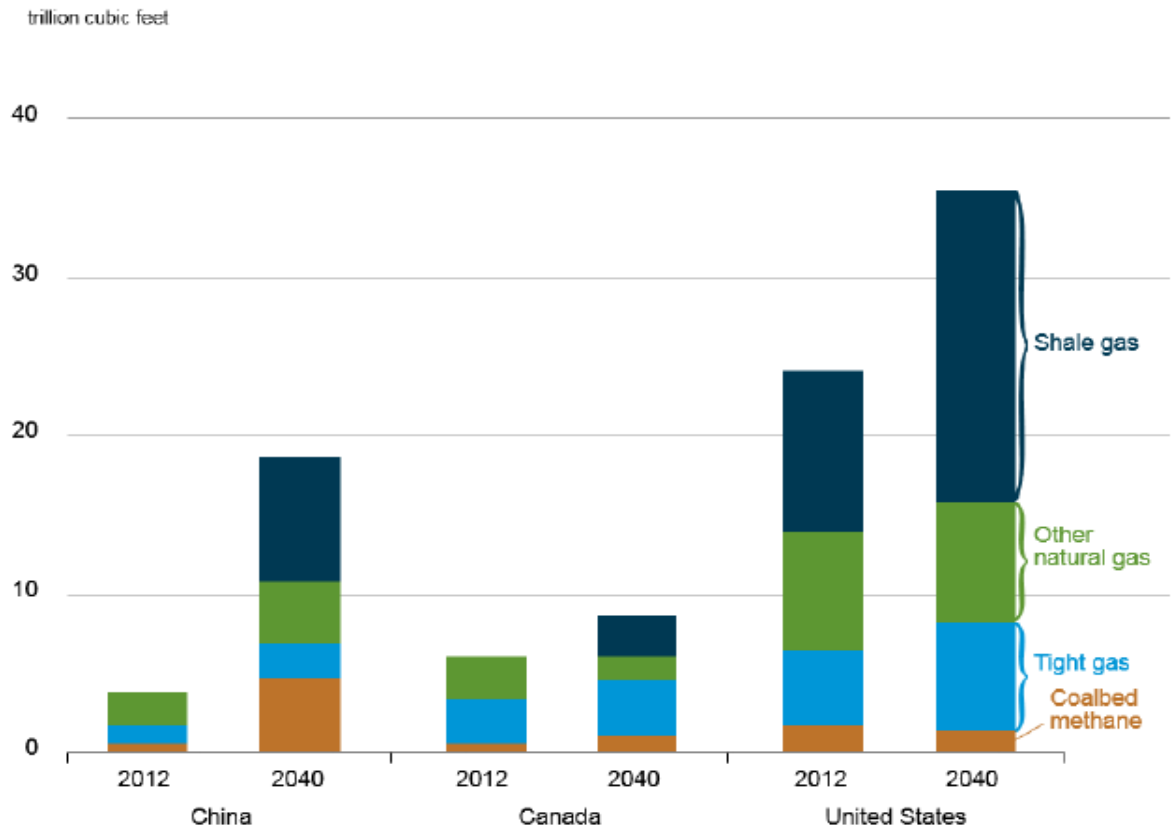


Figure 1.2 Natural gas production by type in China, Canada, and the United State (Cao, 2017)

1.2 Problem Statement

Recently, Karoo gas reserves have been studied, which results showed that the volumes of gas available are not what were previously estimated when the gas reserves were first measured. These findings mean that there is not much gas available, therefore the gas production lifespan for the Karoo shale reservoir will not last for a very long time as previously calculated. When depletion stage is reached, only the adsorbed gas onto kerogen and pores of matrix will be available. Studies show that about 20-80% of gas is adsorbed and is ignored; therefore, there is a need to develop a gas recovery model for depleted gas reservoirs that can include mechanisms to promote gas recovery of adsorbed and diffused gas.

Existing gas flow models need to be modified to include mechanisms that can improve gas recovery and contribute gas production. Most of the gas flow models available use the Langmuir isotherm and follow Darcy's law for low flow rate. Therefore, in this study we look into using BET isotherm for the adsorption mechanism. Recent studies that were done by Yu et al., (2016) showed that the adsorption mechanism is better described using the BET isotherm. Non-Darcy flow will is used instead of Darcy flow since we are dealing with the high-velocity gas flow when gas flows in the fractures system, this effect is usually ignored in most available models.

1.3 Research Aim and Objectives

1.3.1 Aim

This research project aims to develop a modelling of gas recovery from unconventional shale gas reservoir for the depleted gas reservoir to enhanced gas desorption and diffusion mechanisms.

1.3.2 Objectives

The following are set objectives of the research:

- Develop a theoretical gas recovery shale gas model that includes non-Darcy, Knudsen effect correction, adsorption, CH_4 desorption from pore surface and diffusion mechanisms from kerogen for the depleted gas reservoir, adsorption obeying BET isotherm which represent CO_2 injection.

- To simulate the developed model using MATLAB to study the gas recovery by desorption and diffusion mechanisms.

- To investigate how effective the gas recovery is, due to pressure depletion over distance and time.
- Validate the developed model against other existing models

CHAPTER 2: LITERATURE REVIEW

2.1 Shale Gas Exploration

South Africa's geological Karoo Basin covers an area of about 700 000 km^2 and has been discovered to contain natural gas called shale gas. According to assessment studies done in this area, 87% of the surface area it consists of sandstones, mudstones and shale of the Beauford Group. There are estimations that there is a large amount of shale gas, deep biogenic gas and coal bed methane in this area. South Africa has shown interest in this natural gas trapped in deep underground shales of the Karoo Basin. Kock et al. (2017) state the Karoo Supergroup has deposited some 300 to 183 million years ago on the continent Gondwanaland but now referred to as the Main Karoo Basin, shown in Figure 2.1

According to Geel et al. (2013), the studies were done by Decker and Marot (2012) in Whitehill formation of the Ecca group, and they estimated that the Southern Karoo has potential reserves between 32tcf to 485tcf. Recent studies investigated by Kock et al. (2017) concluded that the most realistic resource estimates are between 13tcf to 49tcf, which are lower than previous estimates. Kock et al. (2017) stated that even though these estimates are lower than previously estimated, they still represent a large resource with development potential for the South African petroleum industry. There is concern that the shale reservoir is too shallow to be of commercial interest because the depth of shale should be more than 1500m for safe hydraulic fracturing to avoid any risk of gas escaping. However, they highlighted that even though there's a risk at a depth less than 1000m, any residual gas, desorbed and free gas will remain in place.

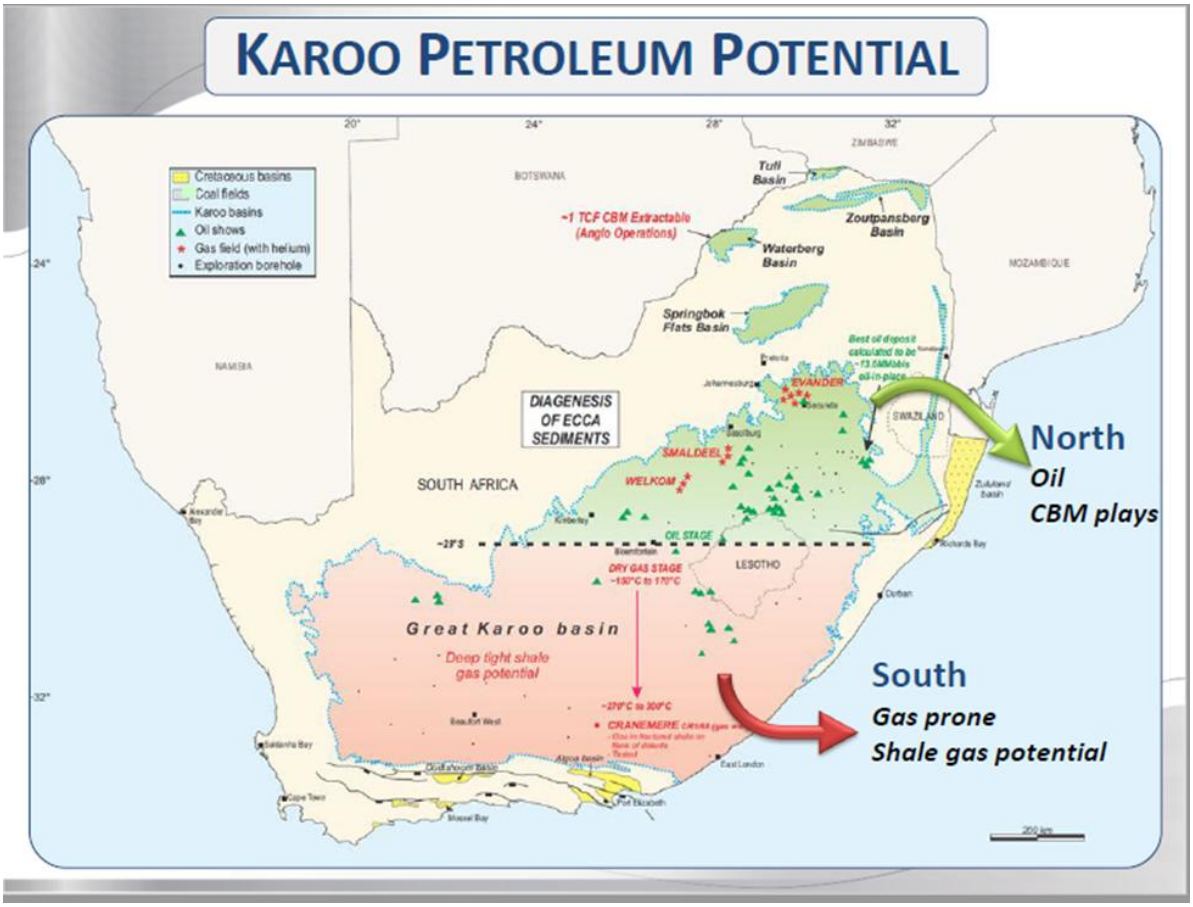


Figure 2.1 Main Karoo basin showing the location of the cores studied (Adams, 2016)

2.2 Horizontal well with Multistage Fracturing Technique

Hydraulic fracturing techniques combined with horizontal well technology is used to effectively and economically to produce oil and gas from shale reservoirs with absolute permeability less than 0.1 md by creating many bigger fractures within the reservoir, which provide the main flow paths into the horizontal well for production. Figure 2.2 shows the overview of how the hydraulic fracking production works whereby gas flows from kerogen feeding matrix (nanopores) by desorbing and diffusing. This gas becomes available as free gas which then flows through microfractures to the production well. Shale reservoirs consist of free gas, dissolved gas and adsorbed gas as shown in Figure 2.2. Free gas is seen in the nanopores, micropores and microcracks within inorganic matter. Adsorbed gas and dissolved is seen in the kerogen grains

within the organic matter. All these pores and fractures develop a gas transport mechanism whereby free gas present in fractures can flow through the network to the production well, then the gas available in the matrix transfers into the fractures to supply the production well. After this process, there is no more free gas available, but only adsorbed and dissolved gas. In Cao (2017) paper, Curtis stated that due to the presence of kerogen and the large surface area in these reservoirs, the content of adsorbed natural gas in shale rocks could be up to 20-80%. This adsorbed gas is known to be present on the surfaces of the kerogen nanopores and grains within organic matter. The most pores of kerogen are nanoscale ranged from a few nanometers to hundreds of nanometers, and the pores or cracks in inorganic matters are mostly microscales as shown in Figure 2.2. The dissolved and adsorbed gas within kerogen desorb and diffuse out and flow into matrix macropores and microcracks, then through hydraulic fractures to the production well as seen in Figure 2.3.

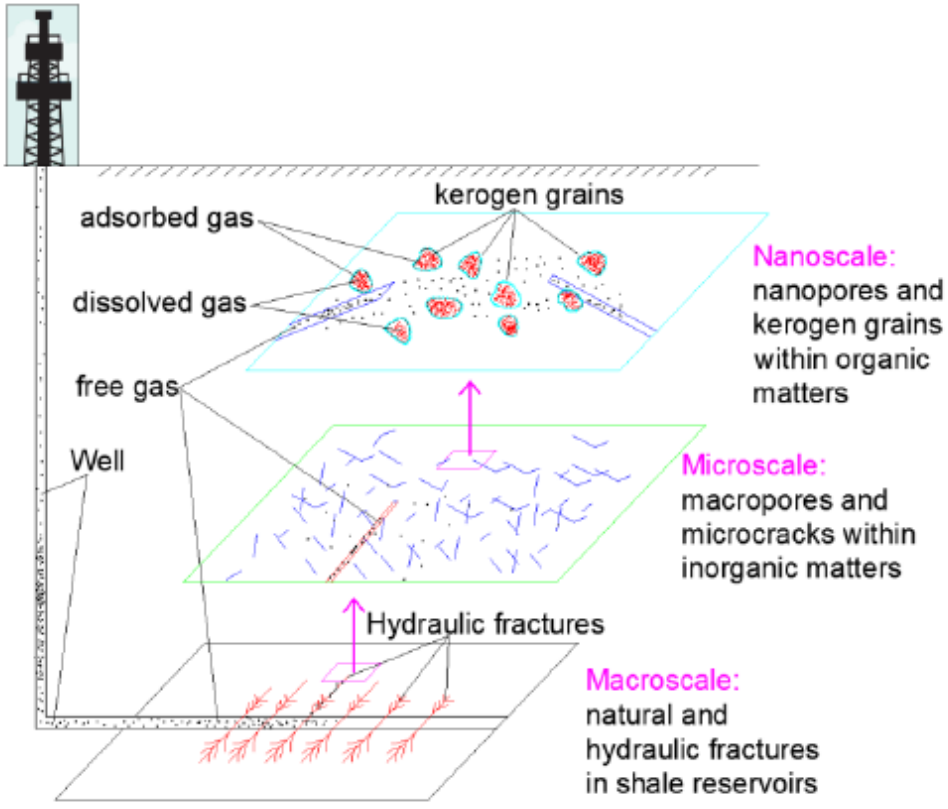


Figure 2.2 Gas production in shale gas reservoirs within different scales (Cao, 2017)

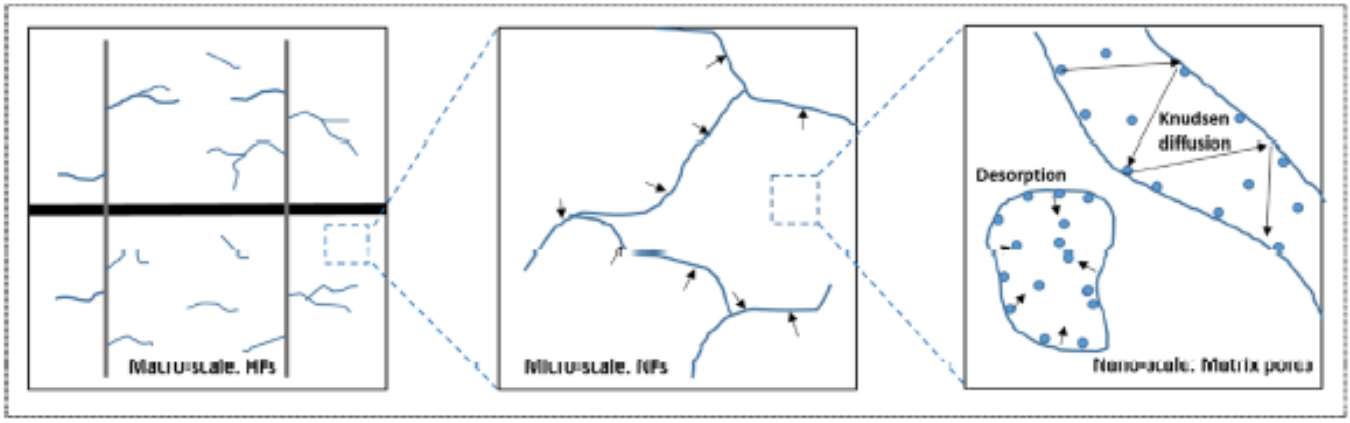


Figure 2.3 Illustration of gas flow from nanoscale to macroscale (Zhang, Xu, & Jiang, 2017)

Hydraulic fracturing is an important completion technology for the development of unconventional reservoirs with low permeability to improve productivity and recovery. Zhang (2014) stated that stimulation technique used after horizontal drilling is used to eliminate formation damage by pumping a large volume of fracturing fluids into the wellbore to stimulate the flow of oil and gas by increasing pressure. This technique creates a pressure difference between the wellbore pressure and the original reservoir pressure. Eventually, this pressure difference will cause stress that will exceed the stress needed to break the rock apart forming a fracture and also connecting pores. Furthermore, this fractures the rock, creating pathways in the reservoirs which the oil or gas can flow to the wellbore to enable efficient and economical production. Figure 2.4 and 2.5 are a zoomed-in schematic representation of hydraulic fracturing, showing gas injection and oil/gas production, respectively. The main idea behind hydraulic fracking is to interconnect all the pores containing free gas to create a fracture path for the gas to flow out to the production well. Figure 2.2 and 2.3 describes this technique whereby we can see horizontal well drilling with hydraulic fractures created fracture networks on shale reservoir rock for gas to flow. We can also see microspores and microcracks being interconnected by the fractures to allow free gas to flow from kerogen and inorganic matter. Every shale reservoir is unique, and the stimulation and completion method should be decided based on its individual petrophysical properties (Khan, 2009).

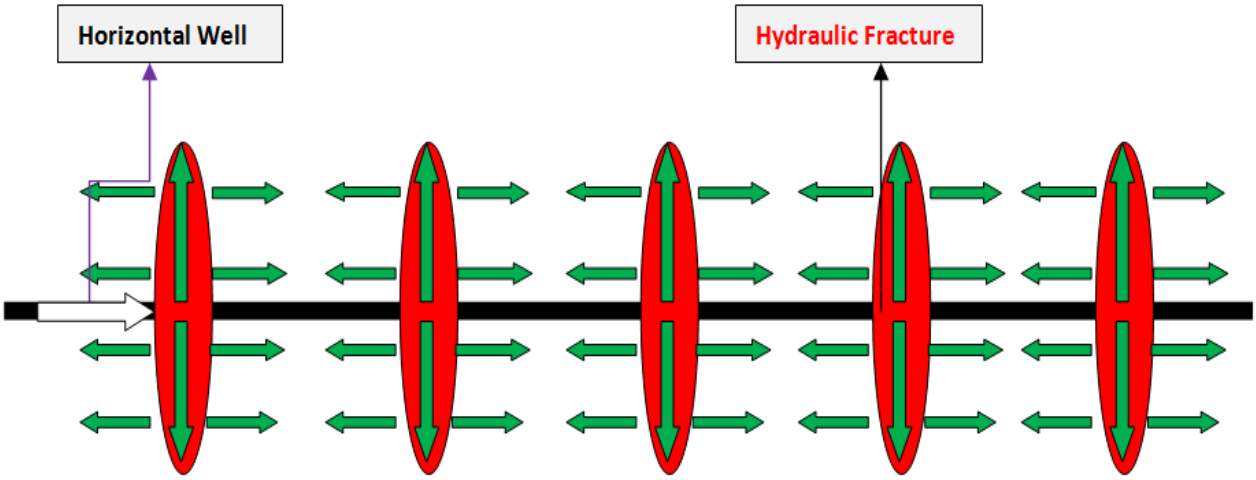


Figure 2.4 Gas injection schematic in horizontal well with multi-hydraulic fractures (Wan, 2013)

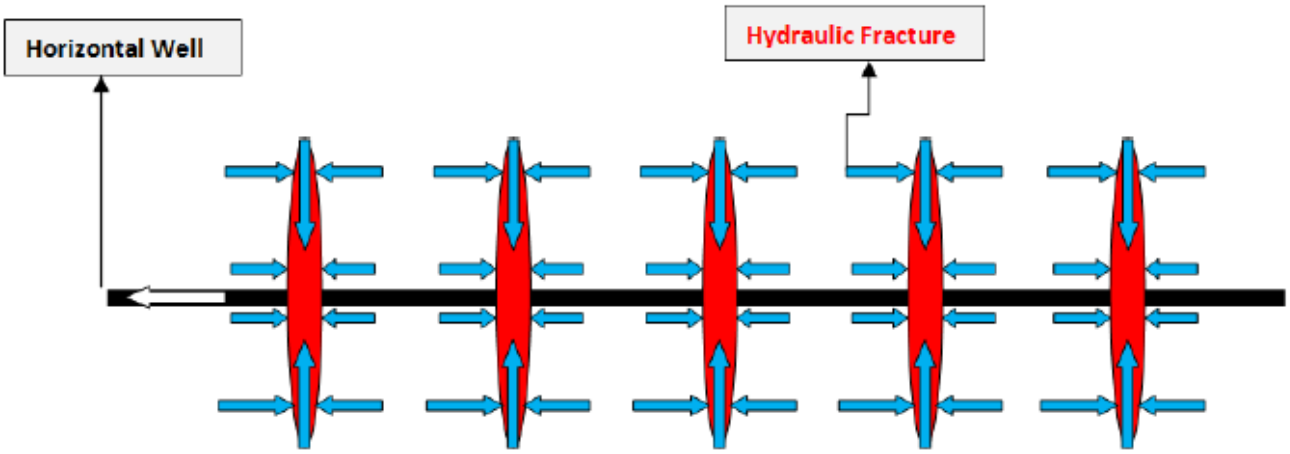


Figure 2.5 Well production schematic in horizontal well with multi-hydraulic fractures (Wan, 2013)

2.3 Shale gas flow

Gas in shale reservoirs is present both in the naturally occurring microfractures and adsorbed onto kerogen and surface of shale matrix. According to Berawala (2015), gas in shale reservoirs is stored in three different ways:

- Free gas in pores and fractures
- Adsorbed gas onto organic matter and clay minerals in the matrix
- Dissolved gas onto kerogen

The total amount of gas in a shale gas reservoir becomes the sum of free gas, adsorbed gas and dissolved gas. Figure 2.6 shows the gas distribution in shale where we can see adsorbed gas, dissolved gas onto kerogen and matrix. Free gas is seen available in the matrix and fractures. According to Berawala (2015), free gas is considered to be present between the region of cube and sphere, whereas as the size of the sphere gives the amount of adsorbed gas which is pressure depended given by Langmuir's isotherm. This statement agrees with Li (2016), stating that shale is characterised as a dual-porosity medium which includes primary porosity and secondary porosity. The primary porosity is known to store the bulk of the natural gas in both adsorbed and as free gas states. Furthermore, they stated that due to the nano-scale porosity, mass transport in this system is dominated by diffusion, driven by the concentration gradient. The secondary porosity is known to be the natural fracture of the rock which has little gas stored as a free gas state. Mass transport in fracture system is dominated by advection driven by the total pressure gradient.

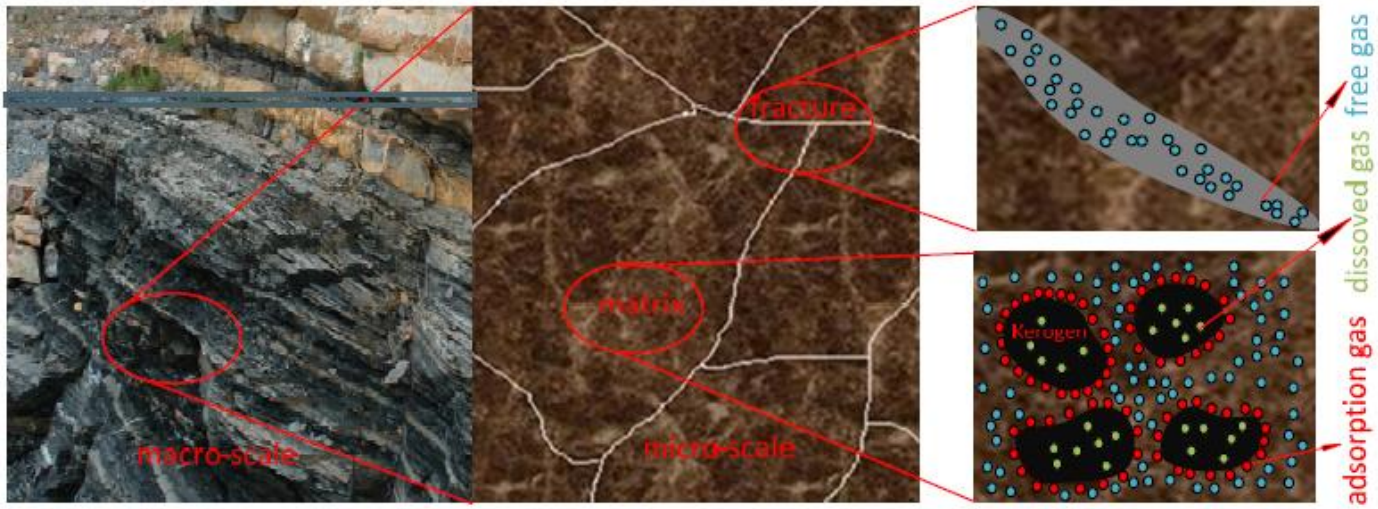


Figure 2.6 Gas distribution in shale strata from macro-scale to micro-scale showing free gas in fractures, free gas and adsorbed gas in the matrix (Guo, 2015).

$$\text{OGIP} = \text{Free gas} + \text{Adsorbed gas} \tag{2.1}$$

$$\text{OGIP} = V_C \left(\frac{\emptyset Sg}{Bgi}\right) + V_S \left(V_L \frac{Pi}{Pi+P_L}\right) \tag{2.2}$$

Where,

V_C is volume of cube (ft^3), V_S is volume of sphere (ft^3), ϕ is porosity of matrix, Sg is saturation of gas, Bgi is gas formation volume factor (scf/rcf), V_L is maximum amount of adsorbed gas, function of the richness or TOC (rcf/scf), P_i is initial reservoir pressure (psi), P_L is Langmuir's pressure at which 50% of the gas is desorbed (psi).

The adsorbed phase is pressure dependent and that when the reservoir is getting depleted, the adsorbed phase is desorbed, therefore increasing gas production. Figure 2.7 illustrates this statement which shows the gas desorption process by diffusion in the matrix system and advection during production Emegwalu (2009). In Figure 2.7 (a) we can see adsorbed and dissolved gas onto kerogen which then desorbs into the matrix as free gas as seen in 2.7 (b). This free gas in the matrix flows out of the matrix to fracture system through macrocracks as seen in

2.7 (c). Then, in 2.7 (d), we see gas being transported by advection to the production well driven by the total pressure gradient in the fracture.

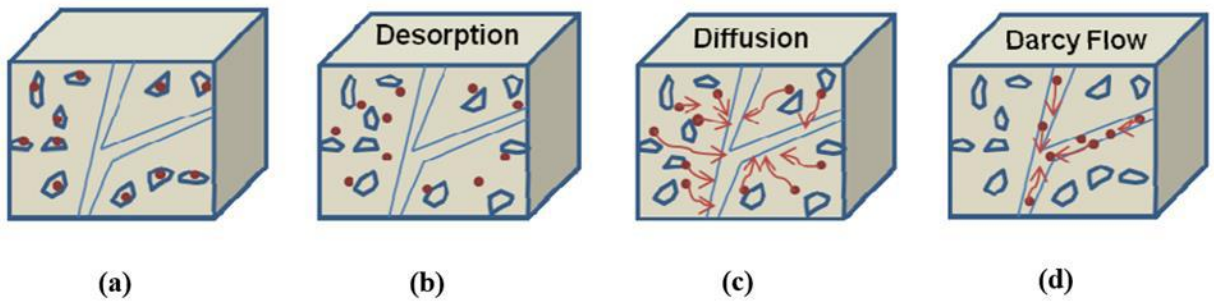


Figure 2.7 Gas flow behavior in the matrix during production (Li, 2016).

According to W. Yu et al. (2016), the main flow mechanisms involved in shale gas reservoir include not only gas advection, but also gas slippage, gas diffusion, and gas desorption which plays a significant part in recovery. Therefore, the diffusivity equation for conventional gas reservoirs should be modified by taking into account all these important flow mechanisms. Yu et al. (2016) studied the contribution of these mechanisms from Marcellus shale and results showed that the contribution of gas slippage, gas diffusion, and gas desorption to gas recovery at 30 years of production compared to when they are not considered are 13%, 17% and 22% respectively. Berawala (2015) studied extensively the adsorption of shale gas mechanism which their simulation results showed that desorption contributes a significant amount of gas to the production. They then concluded their work by stating that adsorbed gas content is given by Langmuir's isotherm and consists of the significant amount of gas which cannot be neglected. However, they highlighted that the transport of gas through diffusion is ignored, as diffusion is a very slow process and the time needed to reach a new balance between adsorbed gas and free gas is so short that it can be neglected. Yu et al. (2016) stated that to simulate gas production in shale gas reservoirs, an accurate model of gas adsorption is very important. Gas desorption may be a major additional gas production and an important factor for gas recovery. Furthermore, neglecting this phenomenon might result in an underestimation of reservoir potential, especially in shale formation with a high TOC (Farah et al., 2017).

2.4 Pore space

Understanding the pore size distribution is very important in evaluating free gas, adsorbed gas and flow characteristics of the shale matrix. According to Guo (2015) pore distribution and morphology of conventional and unconventional reservoir are different, with unconventional shale reservoir having a higher number of nanopores than conventional. Therefore, the exposed surface area in shale reservoir is larger than those in the conventional reservoir, which leads to more adsorption gas. According to Berawala (2015) , pores are classified into two groups: pores inside the non-organic matter and pores inside the organic matter.

2.4.1 Pores within Organic Matter

These types of pores are to be most abundant in the shale and are associated to the generation of hydrocarbon in-situ from kerogen, their sizes ranging from 1 nm to 10 μm and may arrive to have to 1000 pores in a small portion of organic matter (Emegwalu, 2009). Studies performed estimated that the porosity within the organic matter ranges from 0-25% in weight. A good example is Barnett play, which is known to have 70% of the pore volume which comes from the pores present in the organic matter (Emegwalu, 2009). Kerogen has the feature to be able to store a large amount of gas due to its volume pore, whereby inside free gas and adsorbed gas molecules on the pore wall can be found. The Figure 2.8 shows the morphology of nanopores in organic matter in a nanoscopic level using Scanning Electron Microscope (SEM).

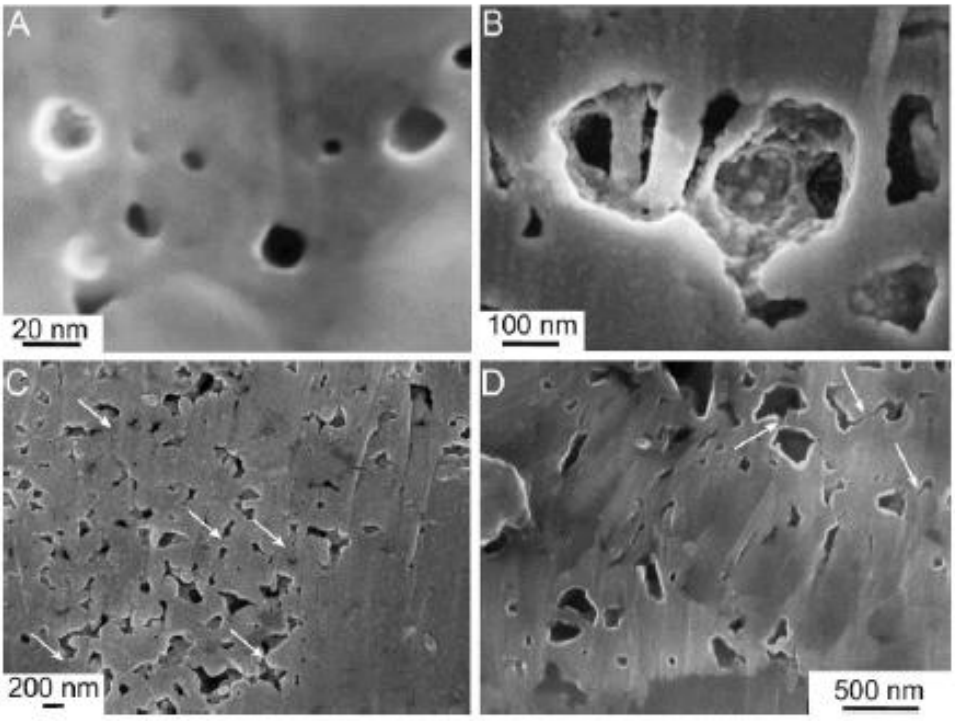


Figure 2.8 Variation in nanopores morphology in organic matter (Guo, 2015)

2.4.2 Pores within Matrix

According to Berawala (2015), pores within the matrix are classified in different forms which consist of intercrystallite pores, intraparticle pores, intragranular pores and pores formed by mineral dissolution.

Intercrystallite pores - These are among flakes and other particles present in the matrix, with size ranging from 0.1 nm to 2 μm. These are known to be abundant in highly pressurised, compacted shale. Or shale rich in clays.

Intraparticle pores - These pores are found within nano-fossil fragments, calcareous mudstone or within framboidal pyrite, with pore size ranging from 0.1 nm to 1 μm.

Intragranular pores – These pores are associated with grain-supported silty laminae or beds within shale. They are known to be larger than pores found in organic matter, with sizes ranging from 10 μm to 20 μm.

Pores formed by dissolution - These pores are created by the dissolution of carbonates, dolomite and pyrite. These are known to be present in smaller quantities associated with secondary porosity, with sizes ranging from 2 μm to 200 μm.

2.4.3 Pore space characterisation

In Berawala (2015), shale production studies, they developed a gas production flow model considering one cell, whereby they assumed that all the kerogen bulk or organic matter is located inside the sphere. Therefore the amount of gas is present only inside the sphere. Furthermore, the space outside of the sphere and inside the cube consists of inorganic matter with micro-fractures where free gas is available. Figure 2.8 illustrate this system. According to Berawala (2015), this assumption is made because the matrix in this cell means both the organic matter or kerogen and the inorganic matter, but because the inorganic matter has much bigger pores, they are classified as micro-fracture. Therefore it is convenient to define pore space inside the organic matter as matrix and that of inorganic matter as micro-fractures. During production, free gas in natural fractures and micro-fracture is produced first, then the free gas in the organic matter or kerogen nanopores feed these fracture networks, the organic matter or kerogen nanopores is in turn fed by adsorbed gas on organic matter or kerogen inside the nanopores surface. The desorption of gas from organic matter or the surface of kerogen driven by a decrease in pressure and diffusion due to the gas concentration gradient.

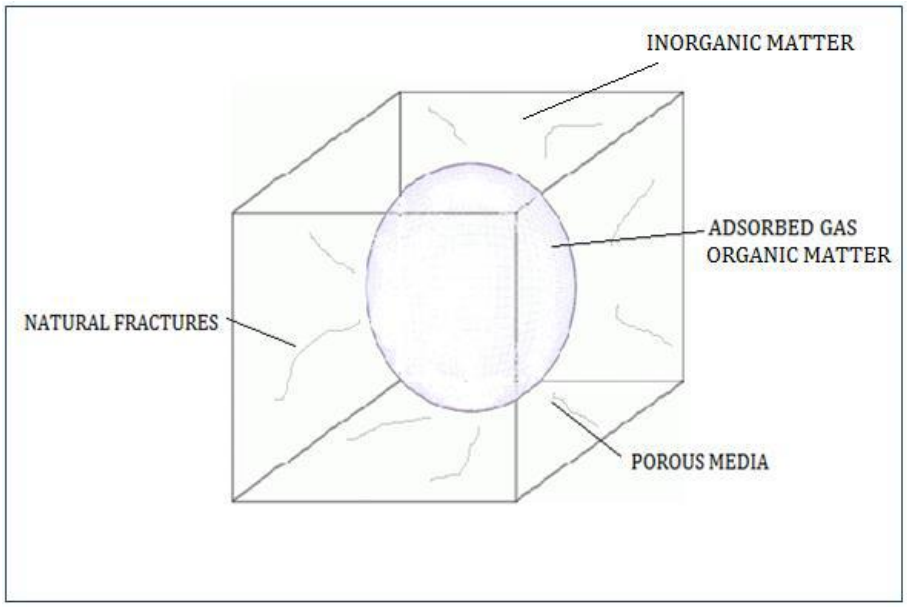


Figure 2.8 3D representation of single cell (Berawala, 2015)

Figure 2.8 and 2.9 show a schematic representation of the gas flow inside the organic matter nanopores towards the network of fractures. According to Swami (2013) due to adsorbed gas, the effective hydraulic dimater of the pore can be be very small compared to actual dimater and as soon as the gas starts to desorbs, the pore diamater increases significantly. Furthermore, this reduces tortuosity and causes extra slippage at the boundary, thereby increasing the matrix permeability many folds.

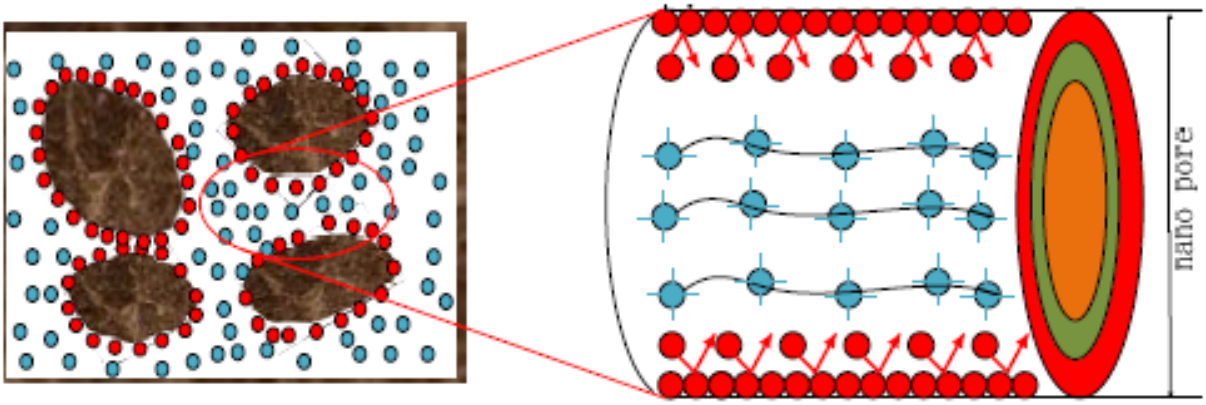


Figure 2.8 Gas flow mechanism in a nano pore. Red represents Knudsen diffusion, and blue represents viscous flow (Guo, 2015)

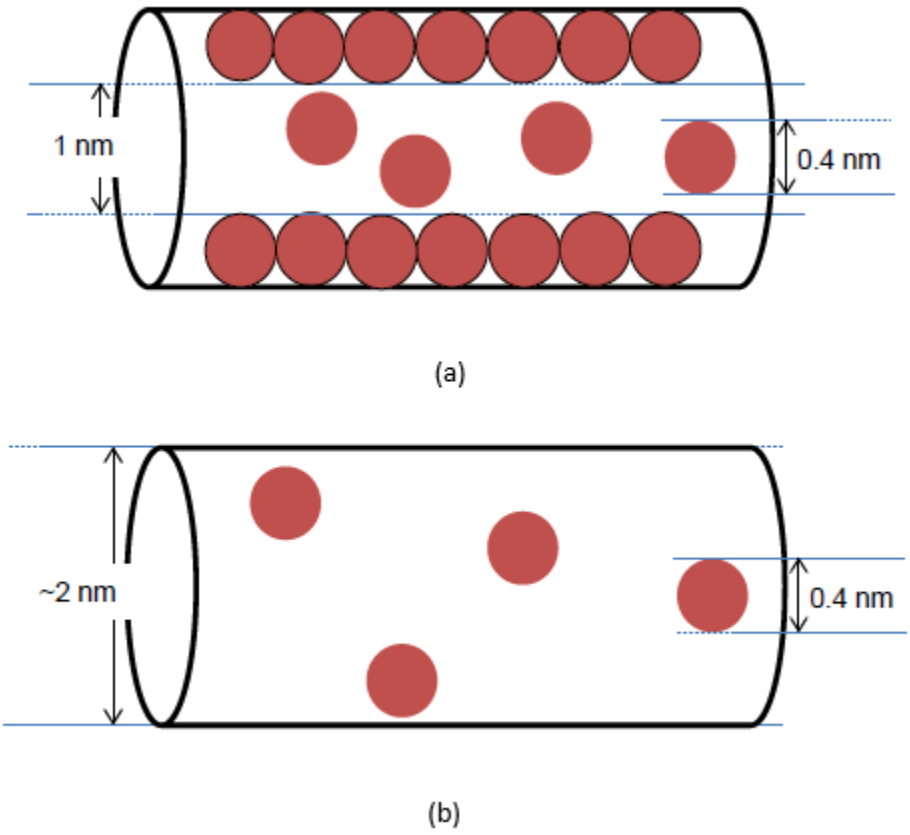


Figure 2.9 Pore diameter change due to methane gas desorption; (a) adsorbed and free gases inside a nanopore, (b) increased pore diameter due to desorption (Swami, 2013)

2.5 Diffusion

Molecular diffusion in known as the process by which matter is transported from one part of a system to another as a result of random molecular motions. This movement is caused by molecules concentration difference, from high concentration to lower concentration. According to W. Yu et al. (2016), Figure 2.10 (a) and (b) show Darcian flow due to pressure and Fickian flow due to the concentration gradient, respectively. The green arrow represents the Darcian flow direction, and the small arrows indicate random flow. In Figure 2.10(a) it can be seen that diffusion is driven by pressure difference ($p_1 > p_2$) and there is no concentration difference due to equal densities ($\rho_1 = \rho_2$). However, in Figure 2.10 (b) we see both Darcian flow and Fickian flow driving the diffusion. Both in Figure 2.10 (a) and (b) molecules move from high pressure to low pressure, or molecules move from high concentration to low concentration.

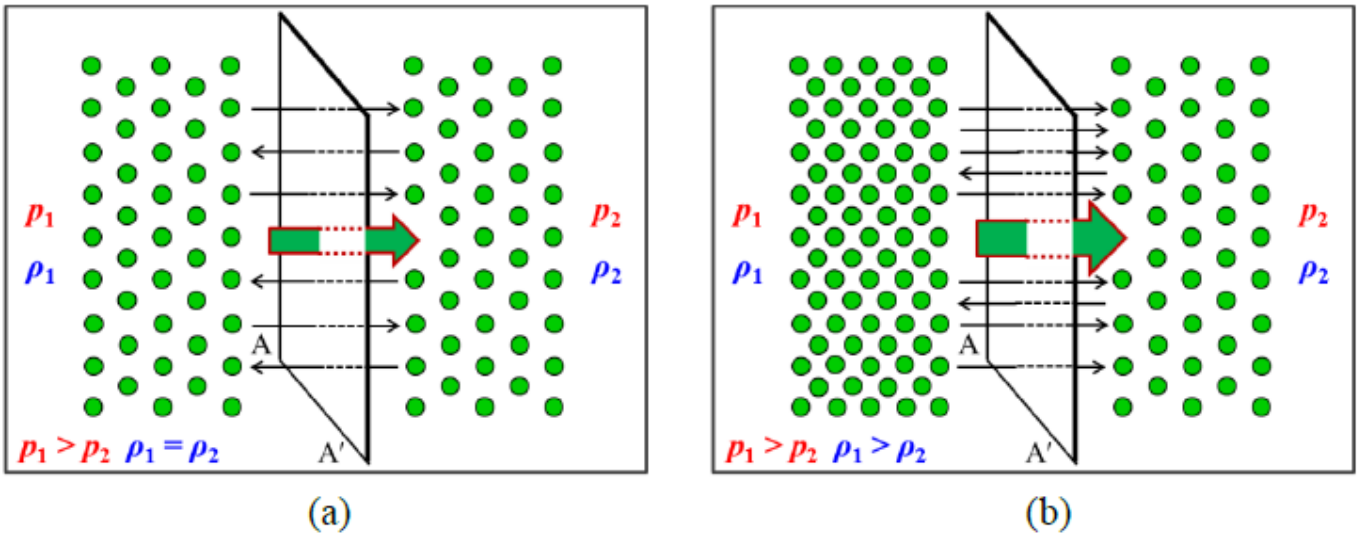


Figure 2.10 (a) Darcian flow due to pressure gradient; (b) Darcian flow due to pressure gradient and Fickian flow due to the concentration gradient (Yu et al., 2016).

According to Chen et al. (2018) due to the multiscale gas transport behaviour in shale, diffusion plays an important role for gas production from the matrix, which is the intermediate link between gas desorption from organic matter and gas flow in the large pores or fractures. Therefore, an accurate and comprehensive understanding of shale gas diffusion behaviour is significant for efficient development of shale gas. There are different types of gas diffusion in

porous media, which could be the combination of bulk diffusion, Knudsen diffusion and surface diffusion acting individually or simultaneously. These mechanisms are shown in Figure 2.11, where we see in 2.11(a) free molecular diffusion or Fick diffusion. These dominate the large pores and high-pressure conditions and is bulk-gas diffusion; 2.11(b) Knudsen diffusion, molecule-pore wall collisions dominate the gas transport and is bulk diffusion; 2.11(c) surface diffusion, transport of adsorbed molecule layer significant for strong adsorbent or small pore, therefore is dissolved gas diffusion; and 2.11(d) configuration diffusion which is the dissolved gas diffusion (Chen et al., 2018)

According to Chen et al. (2018) Knudsen diffusion and Free molecular diffusion usually exist simultaneously and therefore are considered simultaneously for bulk gas diffusion. However, surface diffusion or configuration diffusion it could occur simultaneously with two other kinds of bulk gas diffusion and its contribution to the total gas flux is usually not neglected in the small scale of pores or mid-late production period. Figure 2.12 shows the relationship between multiple pore sizes and diffusion coefficients in shale gas. Shale gas diffusion is lowest at a small pore diameter of about 1-2nm and highest at pore diameter less than 100nm, by the surface diffusion and Knudsen diffusion. The molecular diffusion is seen not playing an important role in gas production for such diameter larger than several hundred nanometers. Therefore due to the size range of shale pores we are dealing with for this work, we will focus on the Knudsen diffusion which is dominant.

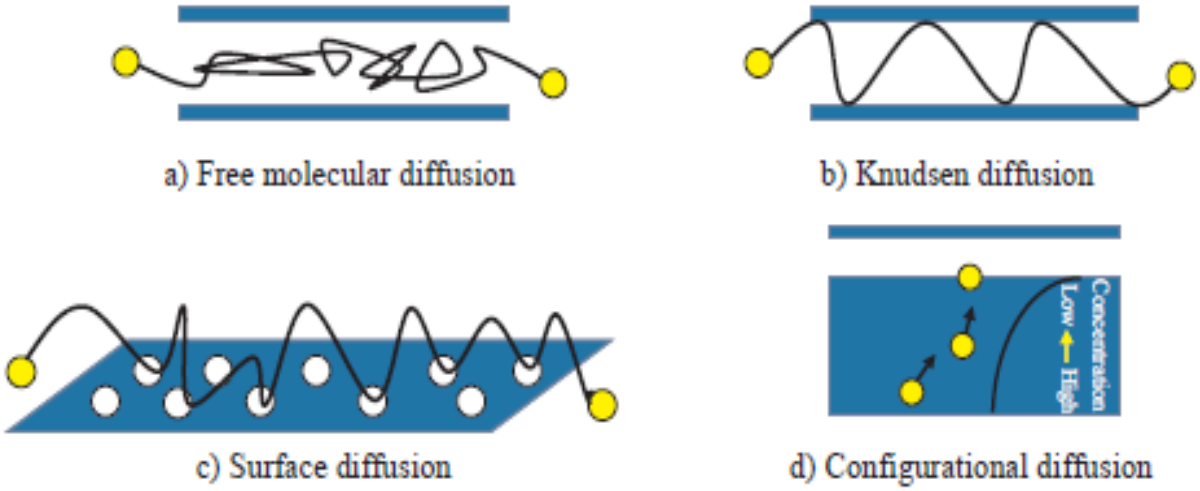


Figure 2 Types of gas diffusion in Shale (Chen et al., 2018)

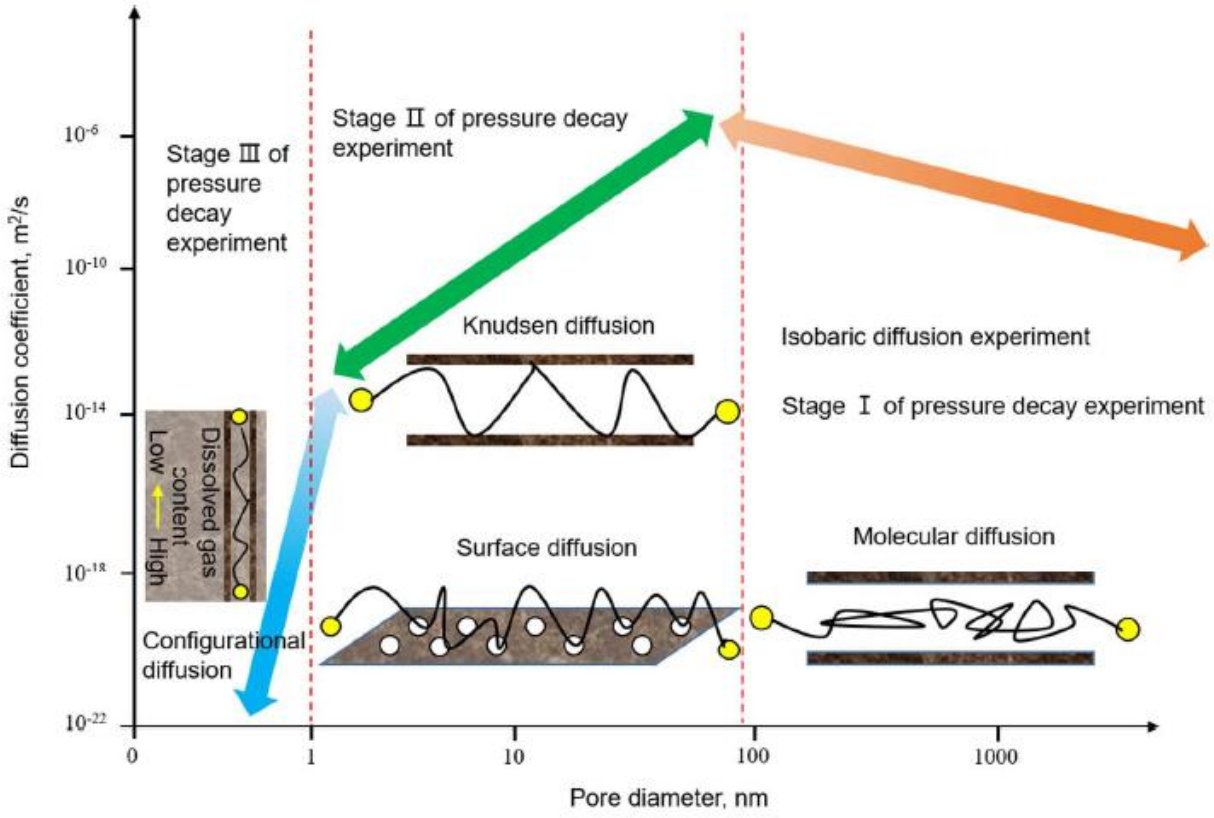


Figure 3: Relationship between the shale gas diffusion capacity and pore diameter (Chen et al., 2018)

Knudsen diffusion (D_k) is given by the following equation (Swami, 2013);

$$D_k = \frac{2r}{3}\left(\frac{8RT}{\pi M}\right)^{0.5} \quad (2.3)$$

Where M is the molecule weight of the gas, r is a radius of the nanopore, R is the universal gas constant (8.314 J/K.mol) and, T is reservoir temperature (K).

Effective diffusion coefficient in the matrix of a porous media can be expressed as:

$$D_m = \frac{\delta}{\tau} \emptyset D_k \quad (2.4)$$

Where D_k is Knudsen diffusion coefficient, δ is a dimensionless constrictivity factor (≤ 1), which accounts for pore size variation along its length caused by small pores, τ is a dimensionless tortuosity factor (≥ 1), accounting for the elongated diffusion path compared to the straight path (Swami, 2013).

According to W. Yu et al. (2016), Dullien, 1979 developed tortuosity estimation equation for the gas flow in porous medium from porosity and gas saturation and can be written as follows;

$$\tau = \frac{1}{\emptyset^{1/3} Sg^{7/3}} \quad (2.5)$$

Dimensionless constrictivity factor developed by Satterfield et al., 1983 can be written as:

$$\delta = (1 - \frac{dgas}{dpore})^2 \quad (2.6)$$

Where $dgas$ is gas molecule diameter and, $dpore$ is the pore diameter.

The gas molar concentration C can be obtained as follows;

$$C = \frac{\rho}{M} \tag{2.7}$$

Where ρ is gas density, M is the molecule weight of the gas. For real gas, gas density is given by;

$$\rho = \frac{pM}{ZRT}$$

2.6 Adsorption/desorption

Natural gas in reservoirs is available in both as free gas, adsorbed gas and dissolved gas, which describe the original gas in place. Emegwalu (2009) stated that adsorbed gas represents significant quantities of total reserves of about 20 to 80 % which cannot be ignored in any model or modelling analysis. It is estimated that desorption of gas contributes around 30 to 50% of the gas produced by shale gas reservoir (Mengal, 2010). This means that as the reservoir is getting depleted, pressure decreases causing adsorbed gas to desorb and dissolved gas to diffuse out, creating free gas for production. According to Berawala (2015) to measure the amount of adsorbed gas and gas content, sorption isotherm is measured in the lab using core samples. Berawala (2015) performed an adsorption study which they used Langmuir isotherm for Barnet Shale to define the relationship between pressure and gas storage capacity of the rock, as shown in Figure 2.13 and 2.14. Figure 2.13 that the adsorbed gas curve follows the Langmuir isotherm and the free gas curve is constructed using the volumetric gas capacity of the reservoir with respect to pressure. Figure 2.14 shows the ratio of adsorbed and free gas changing with respect to pressure and we can see that the adsorbed gas is the dominant contributor to gas production below 2000 psi, 50 to more than 80%, whereas above 2000psi it is significant 50 to 30% (Mengal, 2010).Therefore, this means that at low reservoir pressure the most gas production comes from desorbed gas. Mengal (2010) concluded that ignoring desorbed gas when doing

decline curve or material balance analysis will result in serious errors. Langmuir theory is one of the most used models for the study of adsorption of gases on coal.

Gas adsorption capacity is affected by several factors, such as organic matter, micro-pore structure and mineral composition (Berawala, 2015). Furthermore, organic matter is known to be the most important factor because it affects both the size and the structure of pores in the matrix which affects the amount of surface area that is available for adsorption. Berawala (2015) states that organic matter features include type of organic matter, total organic carbon (TOC) content and thermal maturity which are represented by the Langmuir's volume. Figure 2.15 illustrate the effect of TOC on the adsorbed gas content for the Marcellus Shale.

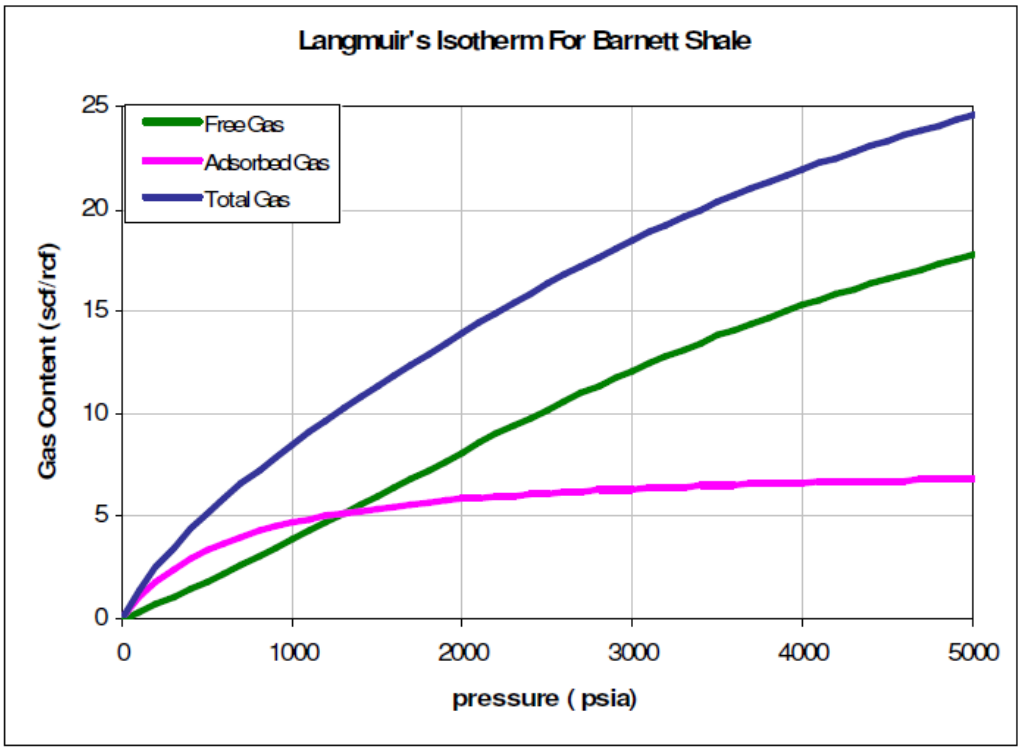


Figure 4 Free, adsorbed and total gas content (scf/rcf) vs pressure for Barnet Shale (Mengal, 2010)

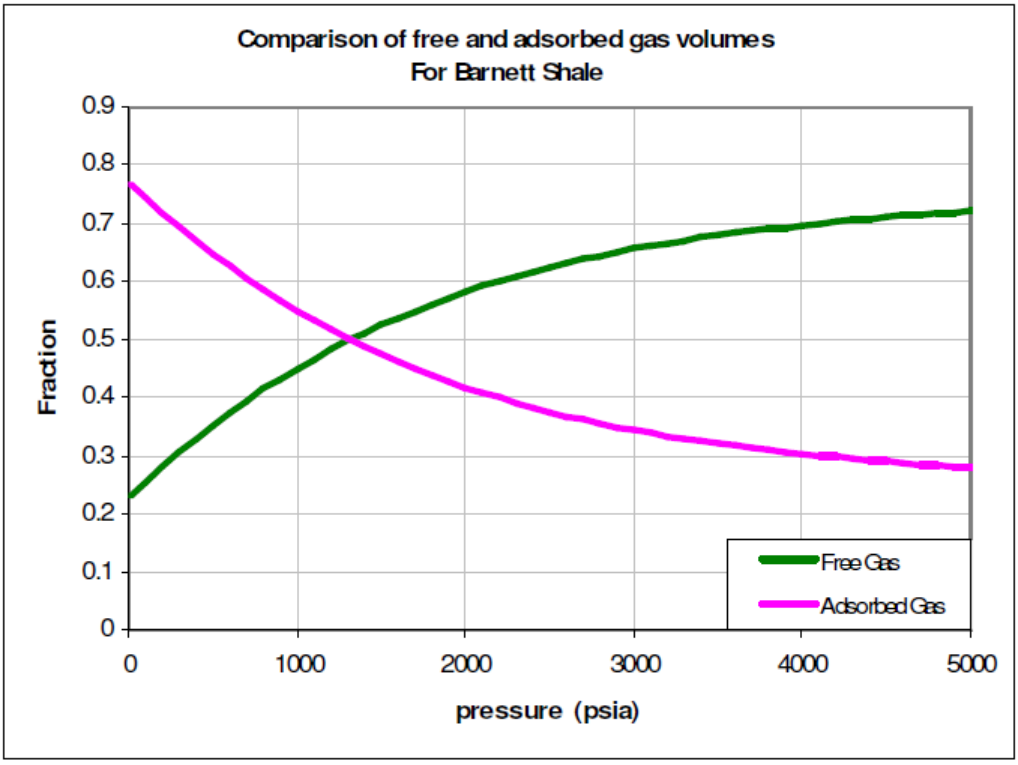


Figure 5 Fraction of adsorbed gas, free gas to total vs pressure for Barnet Shale (Mengal, 2010)

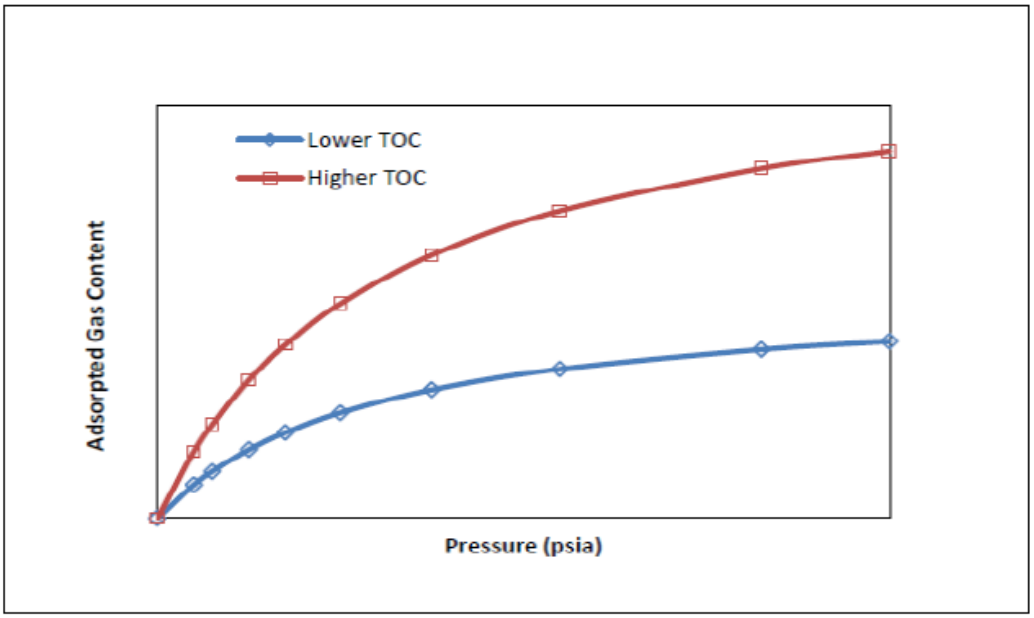


Figure 6 Marcellus Shale adsorption gas content (Berawala, 2015)

The reverse process of adsorption is desorption which is the gas released from matrix surface when the reservoir pressure decreases to critical desorption pressure. According to Berawala (2015), the only time adsorbed gas will start desorbing is when the matrix pressure reaches this lower pressure. This process is slow due to the extremely low permeability of shale formation causing the pressure to drop very slowly, therefore resulting in long-term production. Mengal (2010) stated that the rate of desorption has a significant effect on the production since it reduces the pressure drop in the well and increases the gas production rate. As previously explained in the pore space section that gas is adsorbed on the internal surface of nanopores inside the organic matter or kerogen, which desorbed to form free gas inside the matric pore, then the free gas feed fractures. Swami (2013) states that adsorbed gas at any stage of depletion has its own equilibrium pressure (p_{ad}) which is different from the matrix pressure, during desorption this equilibrium pressure (p_{ad}) remains higher than the matrix pressure due to a time lag caused by sorption time and possibly phase behavior effects of adsorbed gas

Desorption equation can be derived from the Langmuir's adsorbed volume in scf and can be written as (Mengal, 2010):

$$V_{des} = V_L V_b \rho_R \frac{P}{(P+PL)} \tag{2.8}$$

Where, V_b is bulk volume in ft^3, ρ_R is density of shale at initial reservoir pressure in lbm/ft^3

To achieve gas desorption rate scf/sec into total matrix pore space can be found by differentiating the above desorption equation with respect to time we get (Mengal, 2010);

$$\dot{Q} = -\frac{\partial Vdes}{\partial t} = -V_L V_b \, \rho_R \frac{1}{(P+P_L)^2} \frac{\partial P}{\partial t} \tag{2.9}$$

The adsorption/adsorption mechanism was studied in detail by Prusty Harpalani, S. (2004). They performed laboratory tests to investigate the effect of injecting CO_2 into coal partially saturated with methane (CMB) to enhance gas recovery and also investigated preferential sorption mechanism behaviour of coal in the presence of a binary mixture of gases. They performed two tests from different methane pressures, whereby test one results showed that adsorption of methane still followed the Langmuir isotherm and depended only on the partial pressure of methane. However, the second test showed that the actual amount of methane desorbed is greater than the desorption that resulted from the reduction of partial pressure of methane as determined by the Langmuir isotherm in test one, seen in table 1 and 2. Therefore, this shows that the incremental methane produced is because of methane getting preferentially desorbed due to the presence of the highly adsorbing CO_2 gas in rock. Based on the experimental results and analysis of the experimental data Prusty Harpalani, S. (2004) concluded that the recovery of methane could be enhanced by injecting CO_2 into partially saturated coal. Furthermore, the enhancement is probably due to a combination of the effects of partial pressure reduction and preferential sorption.

Table 1. Experimental data of the first injection test (Prusty Harpalani, S., 2004).

Methane Pressure/Partial Pressure (psia)	**CO_2 Partial Pressure** (psia)	**Sorbed Methane** (ml/g)	**Sorbed CO_2** (ml/g)
1332	-	8.5	-
1107	-	7.9	-
900	-	6.8	-
640	-	5.7	-
499	-	5.0	-
204	288	2.1	10.3
83	403	1.0	13.9

Table 2. Experimental data of the second injection test (Prusty Harpalani, S., 2004).

Methane Pressure/Partial Pressure (psia)	**CO_2 Partial pressure** (psia)	**Sorbed Methane**(ml/g)	**Sorbed CO_2** (ml/g)
1356	-	8.2	-
1125	-	7.6	-
905	-	6.3	-
487	-	5.0	-
204	165	3.7	6.4
86	244	1.2	9.9

2.7 Langmuir and BET Isotherm

The most commonly applied gas adsorption model for shale gas reservoirs is the classic Langmuir isotherm, which is based on the assumption that there is a dynamic equilibrium at constant temperature and pressure between adsorbed and non-adsorbed gas (Yu et al., 2016). Langmuir isotherm assumes that there is only a single layer of molecules covering the solid surface, as seen Figure 2.16(a), while BET isotherm assumes adsorbed gas is in multilayer as seen in Figure 2.16(b)

The Langmuir isotherm is defined by:

$$V = \frac{V_L P}{P + P_L} \tag{2.10}$$

Where, V is gas content or Langmuir's volume in scf/ton (standard volume adsorbed per unit rock mass), V_L is maximum amount of adsorbed gas, function of the organic (or TOC), P is reservoir pressure, P_L is Langmuir's pressure, the pressure at which 50% of the gas is desorbed.

The main assumptions of the Langmuir theory are (Prusty Harpalani, S., 2004):

- Every adsorbed molecule is held at definite, localized site
- Each site can hold one and only one molecule
- The surface of the adsorbed is energetically homogeneous

According to Yu et al. (2016), at high reservoir pressures, one can expect that natural gas should sorb on the organic carbon surfaces forms multimolecular layers, which means that Langmuir isotherm may not be a good approximation of the amount of gas sorbed on organic carbon-rich mudrocks. Therefore, multilayer sorption of natural gas should be expected on organic carbon surfaces, and the gas adsorption isotherm type II (BET) should be a better choice. The BET isotherm is a generalisation of the Langmuir isotherm to multiple adsorbed layers, as seen in Figure 2.16(b).

The BET isotherm is defined by:

$$\nu(p) = \frac{\nu_m C p}{(p_0 - p)[1 + \frac{(C-1)p}{p_0}]} \tag{2.11}$$

Where p_0 is the saturation pressure of the gas, ν_m is the maximum adsorption gas volume when the entire adsorbent surface is being covered with a complete monomolecular layer, and C is a constant related to the net heat of adsorption, which is defined below as:

$$C = \exp\left(\frac{E_1 - E_L}{RT}\right) \tag{2.12}$$

Where E_1 is the heat of adsorption for the first layer, and E_L is for the second and higher layers and is equal to the heat of liquefaction.

The assumptions in the BET model are (Yu et al., 2016):

- Homogenous surface
- No lateral interaction between molecules
- The uppermost layer is in equilibrium with gas phase

Yu et al. (2016) studied four experimental measurements of methane adsorption from the Marcellus Shale core samples and found that the measured adsorption in four samples is better described by the BET isotherm, rather than the Langmuir isotherm. Moreover, they highlighted that this behaviour had not been presented in the literature for shale reservoirs to behave like multilayer adsorption. Yu et al. (2016) also studied the desorption gas recovery by considering the Langmuir and BET isotherms. They then concluded their findings that for the gas desorption behaviour obeying the BET isotherm, the adsorbed gas has a similar contribution to gas production with the free gas at both low and high reservoir pressure. Furthermore, for the field well from Marcellus shale, the gas desorption effect with the Langmuir isotherm contributed to 1.1% - 4.7% of gas recovery at the early time of production (190 days), and 4.3% - 1.5 % of gas recovery at 30 years of production. However, the gas desorption effect with the BET isotherm contributed to 6.3% - 26% of gas recovery at the early time of production (190 days), and 8.1% - 36.5% of gas recovery at 30 years of production.

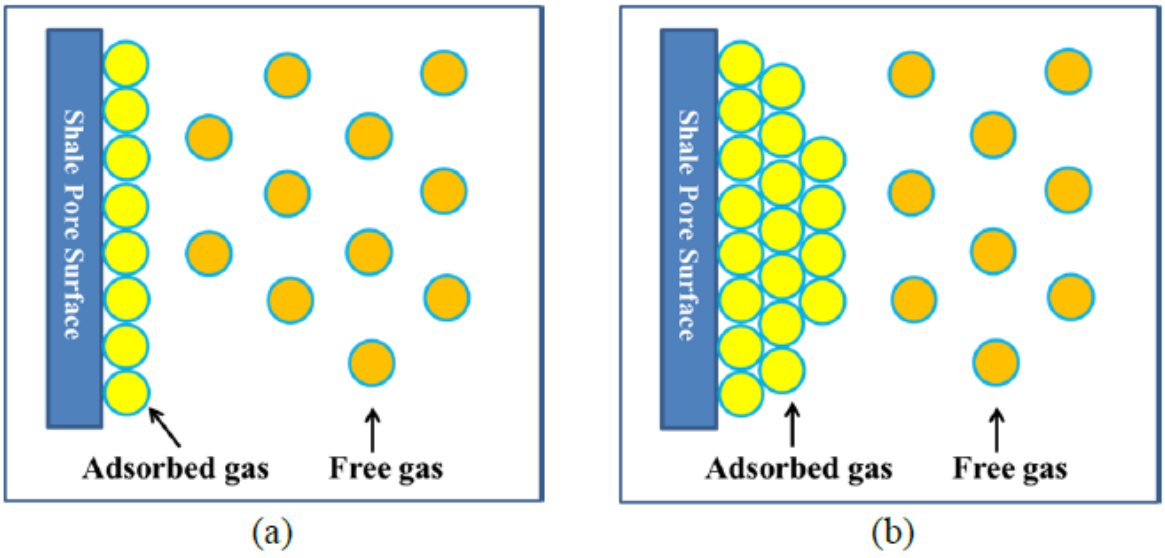


Figure 7: Schematic plot of monolayer and multilayer gas adsorption; (a) Monolayer Langmuir adsorption, (b) Multilayer BET adsorption (Yu et al., 2016).

CHAPTER 3: GAS RECOVERY MODEL DEVELOPMENT

The development of gas recovery flow model for this project is modified from existing models, and includes effects which are not given a lot of attention in most models. Gas is transported from the matrix and kerogen to the fracture by pressure gradient. Therefore, the model is developed in terms of pressure.

3.1 Continuity equation for shale gas

There is a need for the development of new modified gas flow models for unconventional reservoirs to understand and improve gas recovery. The available petroleum flow models are mostly for conventional reservoir obeying Darcy law. Most available models do not consider methods that can improve gas to recover more gas for production. This chapter shows the derivation and modification of existing gas flow model. This model is suitable for depleting or depleted gas reservoirs. Since we are dealing gas we have included non-Darcy flow which is suitable for high-velocity gas flow, the sink term which is related to the rate of methane gas desorption. The derivation focused only on linear flow and x direction to simplify the complexity of the model. The desorption and diffusion terms described by BET isotherm were also included.

The assumptions made to develop this model are as follows:

- Adsorption is defined by BET isotherm
- The reservoir is single-phase flow with gas only
- There is little free gas in fracture system
- The gas desorption mechanism depends on pressure gradient
- Desorption is defined by Langmuir isotherm
- All adsorbed gas at present only inside the pores
- Gas desorption and diffusion takes place inside pores, microcracks and flow only in x-direction.
- Pores are connected to microfracture

- The flow of desorbed gas from the matrix into fractures follows the non-Darcy law.
- The reservoir is isotropic and homogenous with constant height, porosity and permeability

3.1.1 Conservation of Mass

In order to develop a partial differential equation for the flow of fluids in porous media mass continuity, equation of state and equation of motion must be considered (Blasingame, 2008).

The mass continuity equation is described in words as;

$$\begin{pmatrix} rate\ of\ mass\ flow \\ into\ the\ system \\ during\ the\ interval, \Delta t \end{pmatrix} - \begin{pmatrix} rate\ of\ mass\ flow \\ out\ of\ the\ system \\ during\ the\ interval, \Delta t \end{pmatrix} = \begin{pmatrix} rate\ of\ mass\ accumulation \\ in\ the\ system\ during \\ the\ interval, \Delta t \end{pmatrix}$$

The continuity equation is given in mathematical form as (Blasingame, 2008):

$$\nabla \cdot (\rho_g \vec{v}) = -\frac{\partial}{\partial t}(\emptyset \rho_g) \tag{3.1}$$

or

$$\frac{\partial}{\partial x}(\rho_g v_x) + \frac{\partial}{\partial y}(\rho_g v_y) + \frac{\partial}{\partial z}(\rho_g v_z) = -\frac{\partial}{\partial t}(\emptyset \rho_g) \tag{3.2}$$

Where $\vec{v}$ is fluid velocity vector, ρ_g is fluid density, $\emptyset$ is porosity, t is time

Below is a mathematical development of a partial differential equation which describes the flow for a single fluid in a porous media with respect to time, distance and pressure. This derivation is

adopted from Blasingame (2008) from equation 3.1 to 3.18. Assumptions and modifications are made to suit our system and research objectives.

The darcy's law also known as the equation of motion for laminar fluid flow in porous media in vector form is given by

$$\vec{v} = -\frac{k}{\mu}(\nabla p + \rho\vec{g}) \tag{3.3}$$

Where k is effective permeability, μ is fluid viscosity, ∇p is a pressure gradient, $\vec{g}$ is gravity vector.

Since hydraulic fracking production is horizontal flow, there is no gravity force. Therefore we will ignore the term and then the equation becomes;

$$\vec{v} = -\frac{k}{\mu}(\nabla p) \tag{3.4}$$

Combining equation 3.1 and 3.4 gives us

$$\nabla \cdot \left(\frac{\rho k}{\mu}\nabla p\right) = \frac{\partial}{\partial t}(\emptyset\rho_g) \tag{3.5}$$

The next step shows the partial derivation of the diffusivity equation for single phase liquid flow since we assumed that there is no water or oil present. The derivation is in terms of fluid density and pressure, because reservoir pressure change has an effect on density of gas.

The permeability k and the fluid viscosity μ were assumed to be constants. The equation then becomes

$$\nabla \cdot (\rho \nabla p) = \frac{\mu}{k} \frac{\partial}{\partial t} (\emptyset \rho_g) \tag{3.6}$$

The left side of the equation is expanded using the product rule and chain rule, then equation (3.6) became

$$(\nabla \cdot \rho)\nabla p + \rho \nabla \cdot \nabla p = \frac{\mu}{k} \frac{\partial (\emptyset \rho)}{\partial p} \frac{\partial p}{\partial t} \tag{3.7}$$

Chain rule is used for the gradient term, then the first term on the L.H.S of equation 3.7 can be rewritten as

$$(\nabla \cdot \rho)\nabla p = \frac{\partial \rho}{\partial p} \nabla p \nabla p = \frac{\partial \rho}{\partial p} (\nabla p)^2 \tag{3.8}$$

The second term on the L.H.S of equation 3.7 is reduced

$$\rho \nabla \cdot \nabla p = \rho \nabla^2 p \tag{3.9}$$

Substituting both equation 3.8 and 3.9 into equation 3.7, gave the following equation

$$\frac{\partial \rho}{\partial p} (\nabla p)^2 + \rho \nabla^2 p = \frac{\mu}{k} \frac{\partial (\emptyset \rho)}{\partial p} \frac{\partial p}{\partial t} \tag{3.10}$$

On the R.H.S of equation 3.10, product rule is used to the term $\frac{\partial(\emptyset\rho)}{\partial p}$, and the equation became

$$\frac{\partial(\emptyset\rho)}{\partial p} = \emptyset\frac{\partial(\rho)}{\partial p} + \rho\frac{\partial(\emptyset)}{\partial p}$$

Factoring out the $\emptyset\rho$ terms gave the following

$$\frac{\partial(\emptyset\rho)}{\partial p} = \emptyset\rho\left(\frac{1}{\rho}\frac{\partial(\rho)}{\partial p} + \frac{1}{\emptyset}\frac{\partial(\emptyset)}{\partial p}\right) \tag{3.11}$$

Fluid compressibility is related to density and pressure gradient and is given as

$$c = \frac{1}{\rho}\frac{\partial\rho}{\partial p} \tag{3.12}$$

Since we are dealing with real gases compressibility effect must be included.

And the definition of pore volume compressibility is given as

$$c_f = \frac{1}{\emptyset}\frac{\partial\emptyset}{\partial p} \tag{3.13}$$

Substituting equation 3.12 and 3.13 into equation 3.11, we get

$$\frac{\partial(\emptyset\rho)}{\partial p} = \emptyset\rho\left(c + c_f\right)$$

The total compressibility is defined as $c_t = +c_f$, therefore

$$\frac{\partial(\emptyset\rho)}{\partial p} = \emptyset\rho(c_t) \tag{3.14}$$

Substituting this equation 3.14 back to 3.10, we get

$$\frac{\partial\rho}{\partial p}(\nabla p)^2 + \rho\nabla^2 p = \rho\frac{\mu\emptyset(c_t)}{k}\frac{\partial p}{\partial t} \tag{3.15}$$

Dividing through by the fluid density gives

$$\frac{1}{\rho}\frac{\partial\rho}{\partial p}(\nabla p)^2 + \nabla^2 p = \frac{\mu\emptyset(c_t)}{k}\frac{\partial p}{\partial t}$$

Then using the definition of fluid compressibility, we get final equation

$$c\,(\nabla p)^2 + \nabla^2 p = \frac{\mu\emptyset(c_t)}{k}\frac{\partial p}{\partial t} \tag{3.16}$$

The second term on the L.H.S of the equation is expanded using the definition of operator ∇

$$c\,(\nabla p)^2 + \left(\frac{\partial^2 p}{\partial x^2} + \frac{\partial^2 p}{\partial y^2} + \frac{\partial^2 p}{\partial z^2}\right) = \frac{\mu\emptyset(c_t)}{k}\frac{\partial p}{\partial t} \tag{3.17}$$

But for this model, we will only consider gas flow in the x-direction only, therefore we will assume $\frac{\partial^2 p}{\partial y^2}$ and $\frac{\partial^2 p}{\partial z^2}$ is zero, then the equation becomes.

$$c\,(\nabla p)^2 + \frac{\partial^2 p}{\partial x^2} = \frac{\mu\emptyset(c_t)}{k}\frac{\partial p}{\partial t} \tag{3.18}$$

3.1.2 non-Darcy effect

Gas velocity along fracture is so high that non-Darcy flow effect should be considered (Yu et al., 2016). Therefore, the equation will be modified to include non-Darcy effect assuming this effect is taking place in micro-fracture, kerogen and matrix nanopores. The non-Darcy considered is the Forchheimer correction, which takes into accounts inertia effects due to high velocity that may occur in high permeability regions, such as fractures (Wan, 2013). The equation is given as;

$$\nabla p = \frac{\mu}{k}\nu + \beta\rho\nu^2 \tag{3.19}$$

Where ∇p is pressure gradient normal to the area, k is permeability, μ is fluid velocity, ν is fluid velocity, β is the Forchheimer parameter, ρ is the fluid density.

Substituting equation 3.19 into the diffusivity equation 3.18, it then becomes;

$$c\left(\frac{\mu}{k}\nu + \beta\rho\nu^2\right)^2 + \frac{\partial^2 p}{\partial x^2} = \frac{\mu\emptyset(c_t)}{k}\frac{\partial p}{\partial t} \tag{3.20}$$

3.1.3 Klinkenberg effect

Klinkenberg made observations in 1941 that permeability measured for a given sample using a liquid and a gas is not the same. Therefore permeability should always be corrected when gases are used as the fluid. This is corrected with Knudsen number (K_n) which calculated as 0.12 in Appendix A. Correcting the non-Darcy with klinkenberg effect the equation becomes;

$$c\left(\frac{\mu}{k(1+8\alpha K_n)}v+\beta\rho v^2\right)^2+\frac{\partial^2 p}{\partial x^2}=\frac{\mu\emptyset(c_t)}{k}\frac{\partial p}{\partial t} \quad (3.21)$$

Where α is a constant close to 1, K_n is Knudsen number. The calculated Knudsen number value achieved tells us that this gas flow regime is Slip flow because it is in the range of $0.001 \leq K_n \leq 0.1$. The Knudsen number given by (Yu et al., 2016);

$$K_n=\frac{\lambda}{d} \quad (3.22)$$

Where d is the pore diameter, λ is the mean free path of gas molecules, which is defined by (Yu et al., 2016);

$$\lambda=\frac{k_B T}{\sqrt{2}\pi\sigma^2 p} \quad (3.23)$$

Where k_B is the Boltzman constant 1.3805×10^{-23} J/K, T is temperature in K, p is pressure in Pa and σ is diameter of gas molecules.

3.1.4 Sink/Source term

We then include q_g , the source sink term which represents the mass flow into or out of the block for example, liquid flow from a matrix block into a fracture in naturally fractured reservoir, or flow of gas from a coal matrix into a coal cleat. $q_g > 0$ is injection and $q_g < 0$ is

production Berawala (2015).This term is related to the rate of methane gas desorption that obeys the Langmuir isotherm. The equation becomes:

$$c\left(\frac{\mu}{k(1+8\alpha K_n)}v+\beta\rho v^2\right)^2+\frac{\partial^2 p}{\partial x^2}-q=\frac{\mu\emptyset(c_t)}{k}\frac{\partial p}{\partial t} \tag{3.24}$$

For a grit cell/cube containing adsorbed gas, the source term is given by (Berawala, 2015):

$$q_g=\frac{rate\ of\ desorption}{V_b}$$

The rate of desorption used by Berawala (2015) is derived from the Langmuir isotherm desorption equation given by:

$$V_{des}=V_L V_b\ \rho_R\frac{1}{(P+P_L)}$$

Then rate the equation is given as,

$$\dot{Q}=-\frac{\partial Vdes}{\partial t}=\ -V_L V_b\ \rho_R\frac{1}{(P+P_L)^2}\ \frac{\partial P}{\partial t} \tag{3.25}$$

Therefore, the source-sink term becomes,

$$q_g=V_L\rho_R\frac{1}{(P+P_L)^2}\ \frac{\partial P}{\partial t} \tag{3.26}$$

Substituting equation 3.26 into 3.24, we get

$$c\left(\frac{\mu}{k(1+8\alpha K_n)}v+\beta\rho v^2\right)^2+\frac{\partial^2 p}{\partial x^2}+V_L\rho_R\frac{1}{(P+P_L)^2}\frac{\partial P}{\partial t}=\frac{\mu\emptyset(c_t)}{k}\frac{\partial p}{\partial t} \quad (3.27)$$

3.1.5 Adsorption

This term will use the BET isotherm, as Yu et al. (2016) concluded in his findings that the gas adsorption is better described by BET. Furthermore, his finding showed that the gas desorption effect with the BET contribute more than when Langmuir isotherm is used.

The diffusivity equation then becomes

$$c\left(\frac{\mu}{k(1+8\alpha K_n)}v+\beta\rho v^2\right)^2+\frac{\partial^2 p}{\partial x^2}+V_L\rho_R\frac{1}{(P+P_L)^2}\frac{\partial P}{\partial t}+v(p)-\frac{v_m C p}{(p_0-p)[1+\frac{(C-1)p}{p_0}]}=\frac{\mu\emptyset(c_t)}{k}\frac{\partial p}{\partial t} \quad (3.28)$$

3.1.6 Diffusion effect

According to Chen et al. (2018) due to the multiscale gas transport behaviour in shale, diffusion plays an important role for gas production from the matrix, which is the intermediate link between gas desorption from organic matter and gas flow in the large pores or fractures. Therefore it is important to consider this effect to recover gas during production. Gas diffusion for this model commences during gas depletion when critical desorption pressure is reached, which means it is driven by the pressure gradient. Therefore, when diffusion taking place in nanopores to create free gas is considered, the equation then becomes;

$$c\left(\frac{\mu}{k(1+8\alpha K_n)}v+\beta\rho v^2\right)^2+\frac{\partial^2 p}{\partial x^2}+V_L\rho_g\frac{1}{(P+P_L)^2}\frac{\partial P}{\partial t}+\frac{\nu_m Cp}{(p_0-p)[1+\frac{(C-1)p}{p_0}]}+\frac{\delta}{\tau}\emptyset D_k\nabla\rho_g=\frac{\mu\emptyset(c_t)}{k}\frac{\partial p}{\partial t}$$

(3.29)

CHAPTER 4: SIMULATION RESULTS AND DISCUSSION

Gas recovery model for unconventional shale reservoir was developed in Chapter Three. Reservoir simulation was then performed to predict the behaviour of the model using MATLAB Reservoir Simulation Tool (MRST) to solve the partial derivative equation (pde). The MATLAB code written for this project is attached in APPENDIX B. Figures 4.1 and 4.2 are results obtained from the MATLAB simulation software. Figure 4.1 is a 3D representation of the pde behavior in terms of pressure derivative, time and distance and Figure 4.2 is the 2D representation of pressure and time.

The initial pressure for this reservoir system was 3100psi but was denoted as P = 0 on the graph. P > 0 shows increase in pressure, and P < 0 shows decrease in pressure which means that the reservoir is depleting. Analysis of the obtained results of Figure 4.2 showed initially that the pressure increases very quickly up to 2000 days. This could be explained by available free gas in matrix natural fractures and free gas in matrix nanopores feeding fractures, causing pressure to increase. Therefore, at this stage we get high % gas recovery. The gas flow obeyed high velocity non-Darcy flow since we are dealing with gases. During the production pressure eventually reaches optimum, at this stage gas volume recovery becomes steady because there is no more available free gas in fractures and matrix. Thereafter, we start to see reservoir depletion and pressure decreasing overtime and approaching critical desorption pressure, this is seen after 2000 days up to 5000 days. At 5000 days, it can be seen that the reservoir has reached depleted stage since the pressure does not drop any further. At 5500 days, pressure is at the lowest point and this is the critical desorption pressure. We start to see increase in pressure again and this can be assumed to be desorption and diffusion of gas taking place simultaneously form kerogen, feeding the matrix, then fractures. Therefore, the pressure increase after 5500 days showed that free gas is now available for production.

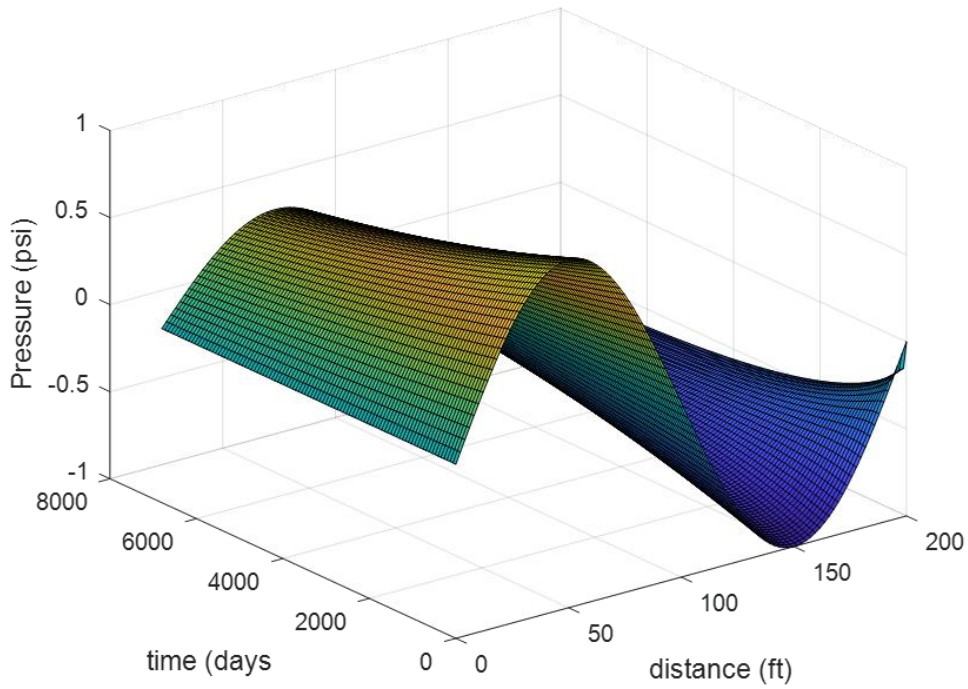


Figure 4.1 Developed model simulation in 3D showing pressure vs time vs distance

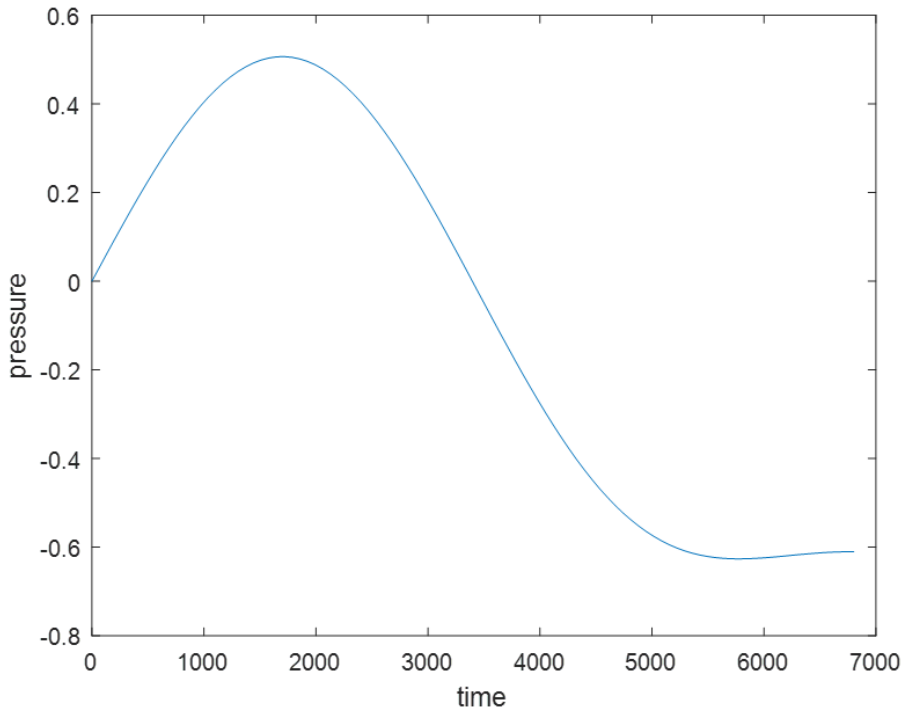


Figure 4.2 Developed model simulation in 2D showing pressure vs time

These numerical model results can be validated with the experimental work of shale gas evolution performed by Javadpour et al. (2007) shown in Figure 4.3, and Swami (2013) shown in Figure 4.4, 4.5, 4.6. The test performed by Javadpour et al. (2007) gives an estimate of gas coming from different regime; free gas in natural fractures, free gas in pores, adsorbed gas and dissolved gas in kerogen bulk. They explained the production profile using statistical models but did not have numerical do validate their work. Figure 4.3 shows their laboratory data results which are plotted as cumulative gas volume versus time. According to Javadpour et al. (2007) curve A corresponds to the gas flow in micropores taking place at the early times, curve B is gas flow in nanopores where Knudsen diffusion is valid, curve C describes gas desorption from the surface of the kerogen/clays pore networks and curve D describes the gas molecule diffusion from the kerogen bulk of clays to the exposed surface showing that the significant amount of gas diffuses out from kerogen bulk. Furthermore, they stated that these curves overlap each other obeying the behavior of the plotted data shown by the long curve, forming a gas evolution curve line.

It can therefore be said that what we seen in Figure 4.2 at initial time from 0 to 5000 days is represented in Figure 4.3 by curve A showing free gas is being produced first. After 5000 days, were pressure has dropped to minimum (critical desorption pressure) is represented by curve C and D which describe gas desorption and diffusion respectively, from the surface of kerogen.

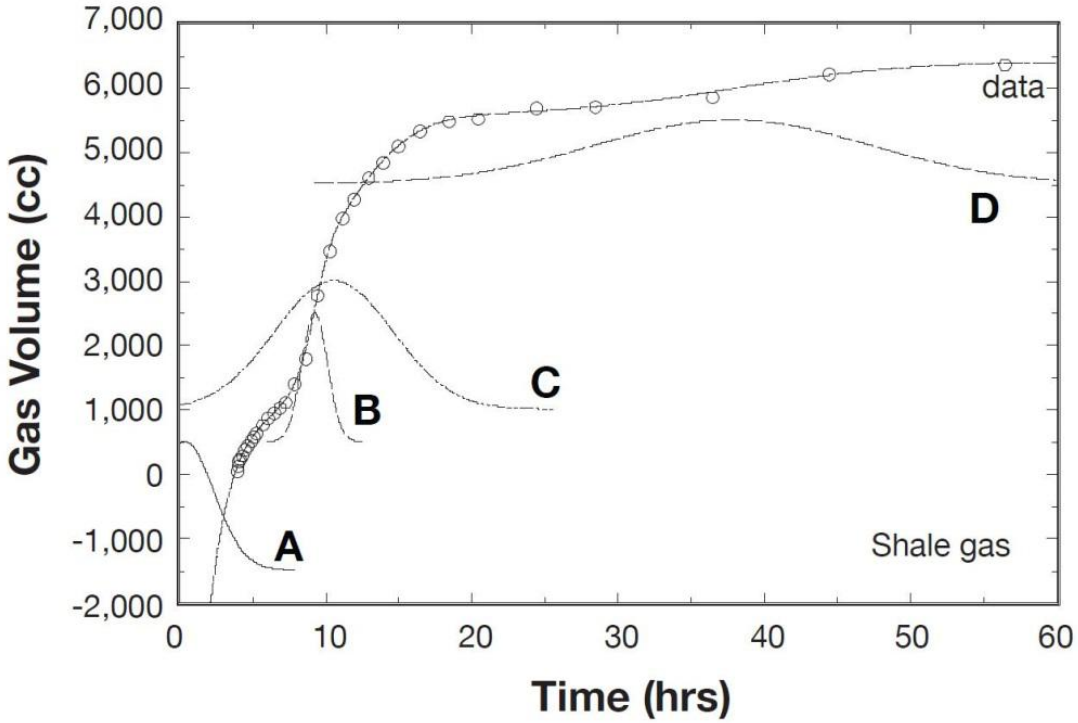


Figure 4.3 Gas evolution and production for shale sample (Javadpour et al., 2007)

Javadpour et al. (2007) laboratory results were later reproduced by Swami (2013), shown in Figure 4.3 and 4.4. In Figure 4.3 we see that at initial stage of production we have gas flow in fractures represented by the blue diamond shaped blocks, after that we have gas flow from matrix nanopores shown by red square shaped blocks, and then desorption is seen taking place shown by the green triangle shaped blocks, followed by diffusion of gas from kerogen bulk represented by the purple cross. This is the order at which gas is produced, from available free gas in the fracture to desorbed gas from the matrix and diffusing gas from kerogen.

The laboratory data curves in Figure 4.4 shows the comparison of individual transport mechanisms that were used to develop the model equation. These curves show how the gas production profile behaves like if one or more gas transport mechanism are excluded or ignore in the model. The blue curve shows a production profile if only fractures system is considered. It can be seen that the free gas in fractures depleted very quickly whereby we see an increase in pressure, meaning fast gas production. Thereafter, the recovery becomes steady because there is only one gas storage availbale. The orange and red curve shows production profile whereby

fracture and matrix (apparent and darcy permeability) are considered, therefore we see that more gas is recovered, because there is two gas storage available which have gas to recover. The green curve shows a production profile when fracture, matrix and desorption are considered, therefore recovery improves because there's gas transport mechanism that is included. The purple curve shows gas production profile when fracture, matrix, desorption are diffusion are considered. Also here, we see that more gas transport mechanisms are included which contribute a lot to gas recovery.

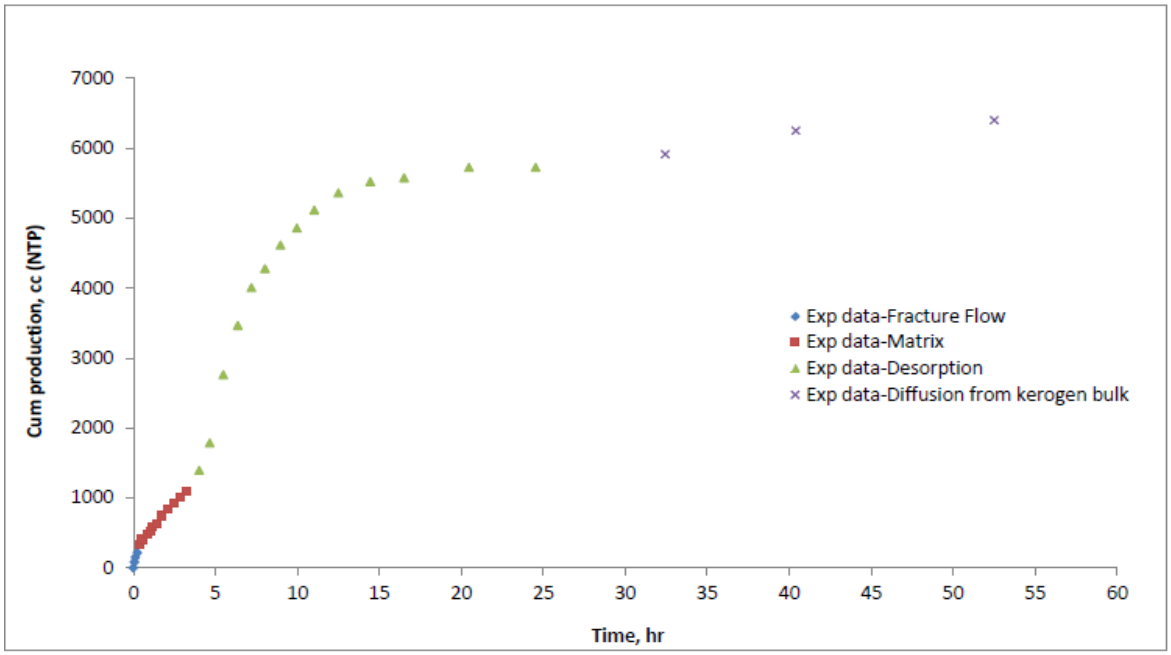


Figure 4.4 Dissociation of experimental data into four flow regimes ; fractures, matrix (nanopores), desorption and diffusion from kerogen bulk (Swami, 2013).

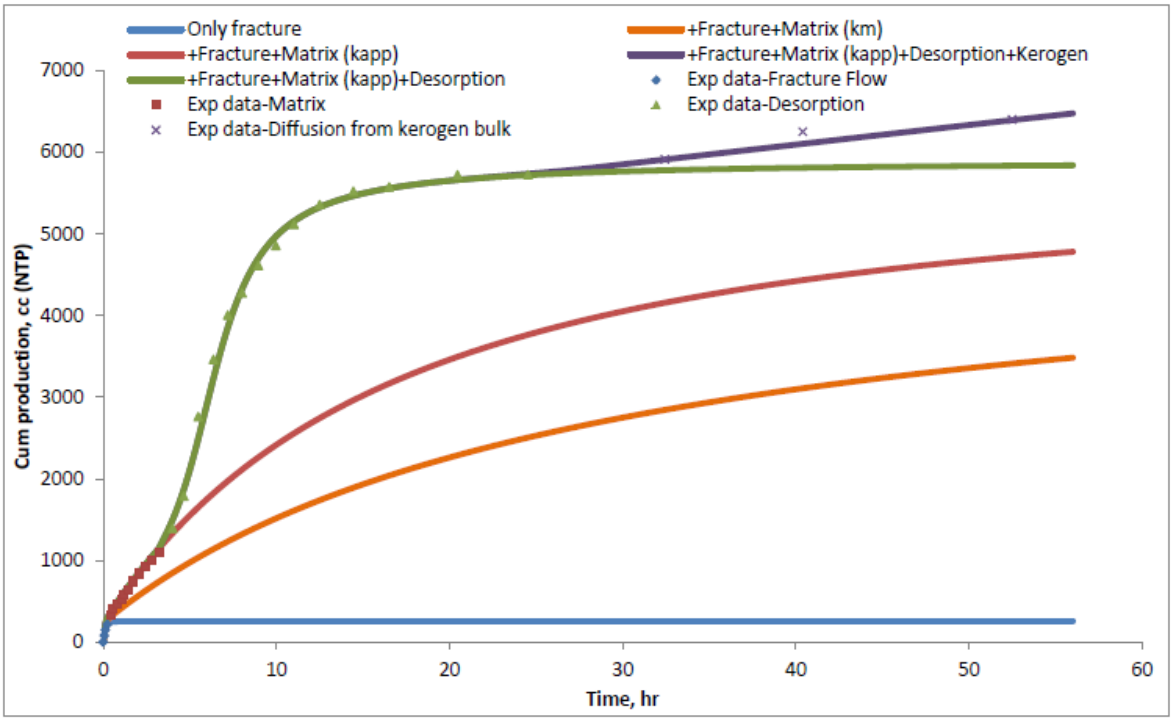


Figure 4.5 Comparison of various storage and transport mechanisms. Also validation with experimental work (Swami, 2013)

Figure 4.6 are simulation results performed by Swami (2013) based on their built numerical model to validate their laboratory results. These result were obtain using real field data and according to Swami (2013) we cannot see well-defined peaks corresponding to different transport mechanisms as observed in the laboratory results. Furthermore, they state that in the field the various storage and transport mechanisms may start contributing at different places at the same time to substantial pressure. Therefore, the peaks observed in the laboratory may get obscured in the field due to the overlapping of the various storage and transport mechanisms.

In this simulation we see that the gas production increases very fast due to increase in pressure to optimum, then drops again hence we see the small peak deeping. At this stage, about 1-1.5 days we can see that free gas available in fractures is depleted. Thereafter, we see a small peak, this stage is critical desorption pressure, whereby we start to see desorption and diffusion from matrix and kerogen taking place and feeding the fractures with gas and therefore causing a steady gas production. This maintains the pressure and thereafter we get a steady gas production as seen in the Figure.

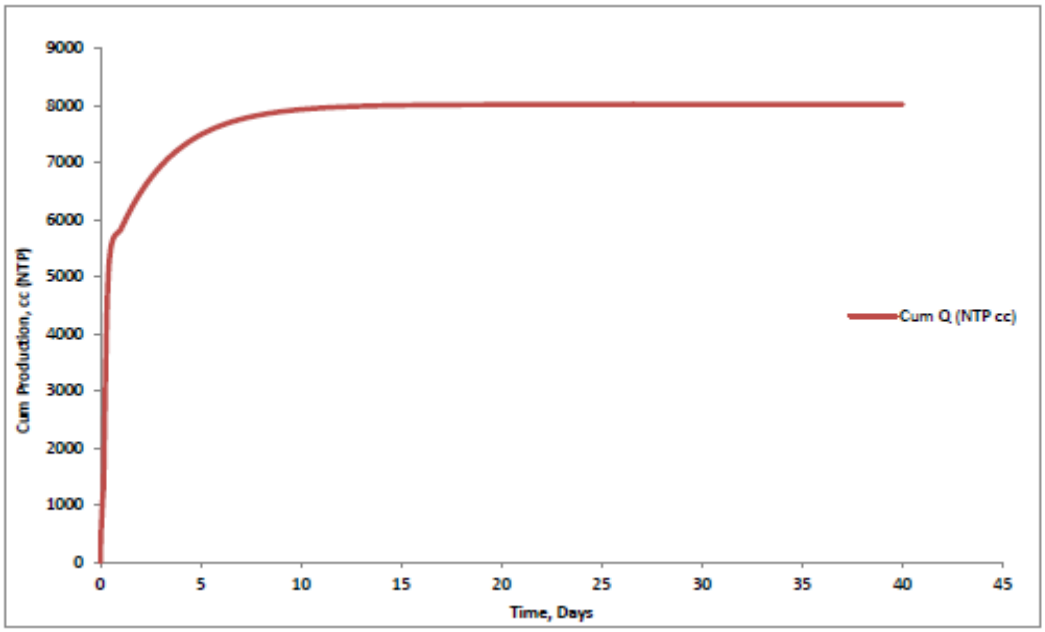


Figure 4.6 Simulation results for cumulative gas recovery after 40 days (Swami, 2013)

Since we know that volume and pressure can be related using the real gas law equation;

$$P = \frac{nRT}{V}$$

$$\therefore P \propto \frac{1}{V}$$

This pressure and volume relationship shows that the simulation results shown in Figure 4.2 can be compared to the laboratory and simulation in Figure 4.3, 4.4, 4.5 and 4.6. This therefore validates our developed model which shows a similar gas production behavior at early stage and during depletion stage. Though in Swami (2013) simulation results the peaks are not well-defined. These could be because the field data used in our model and their model are different, therefore different properties.

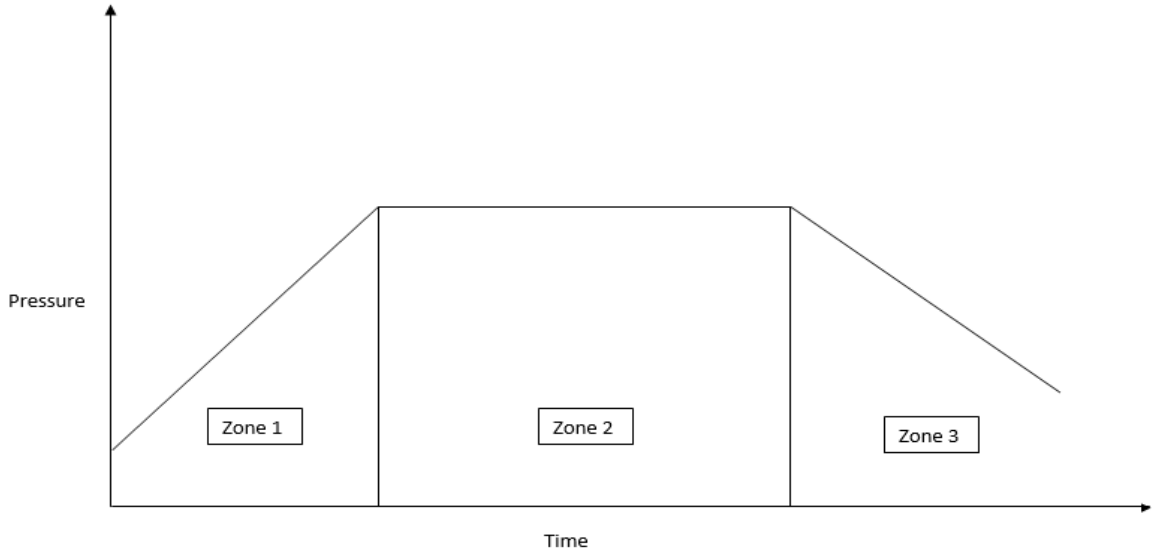


Figure 4.7 Gas recovery profile behavior

Zone One

This part of the recovery profile shows an increase in pressure up to optimum due to the amount of available free gas in the fractures and matrix. The % gas recovery in the early stage of production is high. Similar behavior can be seen in the proposed modeling behavior (Figure 4.2) and Swami (2013) (Figure 4.6). Gas recovery in this zone is spontaneous after fracturing and fluid injection processes. The higher gas production rate (or pressure gradient) is due to the unbalance pressure in the pore space of the reservoir rock. This step can take several hours (20 hours as seen in the investigation of Swami (2013) and Javadpour et al. (2007) or several days (10 days as seen in the investigation of Swami (2013). The pressure gradient and the recovery rate in zone 1 depends on the fracture aperture and the fluid injection rate.

Zone Two

In this zone gas production has reached optimum pressure and gas recovery is steady. At this stage there is no more free gas available in the fractures and matrix. Pressure becomes constant

and is maintained by the desorbing and diffusion gas from the kerogen to matrix, then to the fractures making free gas available again. This zone is the main production period, which last longer (many years) depending on the amount of gas available in the reservoir. Most of the published work showed only the behavior in zone one and two, when the recovery rate reaches the equilibrium. According to Swami (2013) diffusion is comparatively a slow process and is significant. This stage is seen Figure 4.2 and 4.6 but it can be noted that the time taken by then desorption and diffusion in this investigation and Swami (2013) is different. This could be explained by the difference in reservoirs properties and field data used. The area of zone two can be calculated from the predicted amount of the gas in the reservoir and this can also predict the production duration.

Zone Three

This is depletion stage whereby almost all the available gas has been recovered. The pressure decreases and will continue decreasing until more gas has diffused out from kerogen to matrix, then fractures to make free gas available again. If the drop in pressure is due to other factors not related to the depletion of hydrocarbon, investigation on the gas composition, rock pore size and contributions of the number of wells link to the production system should be done. Otherwise, the closure of the production site should commence.

CHAPTER 5: CONCLUSION AND FUTURE WORK

Conclusion

This research has developed a theoretical gas recovery shale gas model for depleted gas reservoir to enhance the recovery of adsorbed and dissolve gas on the shale kerogen surface. The set objectives to achieve the aim were to develop a numerical model and simulation using MATLAB software to study the gas recovery behavior of the developed model. The MATLAB results are then used to investigate how effective the gas recovery mechanisms are, due to pressure depletion over distance and time. The last objective was to validate the results achieved against available numerical or analytical models.

A gas recovery model was developed from the continuity equation, modification were done by including important mechanisms and effects equations like diffusion, sorption, non-Darcy, Knudsen effect. This model was then solved with MATLAB software and a gas recovery production profile was obtained and validated with available gas production profile which showed similar behaviour. In the discussion section, our simulation results were compared to available laboratory and simulation results and they showed similar behavior to our simulations. The theory of shale gas flow and recovery was explained in Chapter Two, whereby it was said that free gas available in natural fractures and micro-fracture in the matrix is produced first, then the free gas in the matrix nanopores feed these fracture networks, the matrix nanopores is in turn fed by adsorbed and dissolved gas on kerogen inside the nanopores surface which take place at later stage of production. This diffusion mechanism was seen in our results at a later stage of production, whereby we observed depleted pressure increases again due to diffusion contribution. This gas production theory matches with our simulation results which we were compared with their results and observed that our results show similar behavior. Therefore, it can be concluded that the developed model to recovery more gas is valid. It can also be concluded that the gas transport mechanism are very important and contribute a lot of gas production to achieve high % recovery.

Future work

- To validate the developed model in the future, core plug laboratory experimental work needs to be designed and performed to see how our experimental work would behave.

- The simulation results seem to be agreeing with the developed model and the theory, but might not be accurate since we assumed and ignored a lot of terms/effects to fit the scope of this project. Therefore, more work needs to be done to make the equation more complex.

- The data used in the simulation was adopted from available U.S Shale reservoirs. These could have affected our results because reservoirs are different and fit their conditions. Some reservoirs are two phase flow, whereby oil and water is present. In this model, we assumed one phase flow. Therefore, to study the developed model to see if it works for the Karoo shale, we need characterize Karoo Shale so that we able to use real data to get accurate results. If not, we need to use data from a very similar shale reservoir to be able to do history matching and get very conclusive results.

- In this research, the permeability and porosity of the reservoir were assumed to be constant, the reservoir is also assumed to be homogenous to simplify the reservoir system. This assumption might not be true representation of what is taking place in kerogen and matrix which could therefore change the behaviour of the model. These properties are the most important in petroleum engineering and need to be characterized to be able to get more realistic results. Especially the apparent permeability which studies show that it is the most important term.

- In the model for the desorption and adsorption mechanisms we used Langmuir isotherm for desorption term, and BET isotherm for adsorption term. The only reason this was done is because BET isotherm required a worked-out derivation of the BET isotherm

equation to get rate of desorption equation which would have exceeded the scope for this project. Therefore, an assumption that Langmuir isotherm describes desorption better was made. In the future, a derivation of desorption described by BET isotherm needs to be derived for consistency regarding the isotherm used.

- Only linear flow and x direction were considered to simply the complexity of the model. Considering that we are dealing with pores and diffusion, radial flow is very important and should be considered.

- In the future gas flow rate need to be studied since we used non-Darcy flow suitable for high velocity gas flow.

.

REFERENCES

Adams, S. (2016). SOUTH AFRICA : Overview of Offshore and Onshore, (May).

Blasingame, T. A. (2008). Reservoir Performance: Diffusivity Equation Development, *3116*(February).

Cao, P. (2017). Impact of Multiphysics Interactions on the Gas Flow Performances in Shale Gas Reservoirs, (April).

Chen, M., Kang, Y., Zhang, T., You, L., Li, X., Chen, Z., Yang, B. (2018). Methane diffusion in shales with multiple pore sizes at supercritical conditions. *Chemical Engineering Journal*, *334*(November 2017), 1455–1465.

Cloete, M. (2010). ATLAS on geological storage of carbon dioxide in South Africa.

Emegwalu, C. C. (2009). Enhanced Oil Recovery : Surfactant Flooding As a Possibility for the Norne E-Segment, (Autumn).

Farah, N., Modelling, F., Unconventional, P., Earth, R., Pierre, L. U., & Marie, E. T. (2017). Flow Modelling in Low Permeability Unconventional Reservoirs Flow Modelling in Low Permeability Unconventional Reservoirs.

Geel, C., Schulz, H. M., Booth, P., De Wit, M., & Horsfield, B. (2013). Shale gas characteristics of Permian black shales in South Africa: Results from recent drilling in the Ecca Group (Eastern Cape). *Energy Procedia*, *40*, 256–265.

Guo, C. (2015). Flow mechanisms and numerical simulation of gas production from shale reservoirs.

Javadpour, F., Fisher, D., & Unsworth, M. (2007). Nanoscale gas flow in shale gas sediments. *Journal of Canadian Petroleum Technology*, *46*(10), 55–61.

Khan, G. (2009). Experimental studies of Carbon dioxide Injection for Enhanced Oil Recovery Technique.

Kock, M. O. de, Beukes, N. J., Adeniyi, E. O., Cole, D., Götz, A. E., Geel, C., & Ossa, F.G. (2017). Deflating the shale gas potential of South Africa ' s Main Karoo basin. *South African Journal of Science*, *113*(9).

Li, Z. (2016). CO_2 and N_2 Injection To Enhance Shale Gas Recovery, (December).

Muhssen, C., & Khan, H. (2013). Techno-Economic Reservoir Simulation Model for CO 2 Sequestration Evaluation, (March).

Prusty Harpalani, S., B. K. (2004). A Laboratory Study Of Methane/CO2 Exchange In An Enhanced CBM Recovery Scenario. *Proceedings of the Int. CBM Symposium*, (January 2004).

Romero-zerón, L. (2012). Advances in Enhanced Oil Recovery Processes. *Introduction to Enhanced Oil Recovery (EOR) Processes and Bioremediation of Oil-Contaminated Sites*, 1–43.

Swami, V. (2013). Development of a "Quad Porosity"Numerical Flow Model for Shale Gas Reservoirs.

Mengal, S. A. (2010). Accounting for Adsorbed Gas and Its Effect on Production Behavior of Shale Gas Reservoirs Accounting for Adsorbed Gas and Its Effect on Production Behavior of Shale Gas Reservoirs. *Analysis*, (August).

Vidolova, M. (2014). Modelling of Gas Production from Tight Shale Formations: An Innovative Approach, 146.

Vincent, C. J., Hicks, N., Arenstein, G., Tippmann, R., Van Der Spuy, D., Viljoen, J., … Naidoo, Y. (2013). A Study into the Viability of Mineral Carbonation as a means of CO2 Sequestration in South Africa, 2013.

Wan, T. (2013). Evaluation of the EOR Potential in Shale Oil Reservoirs by Cyclic Gas Injection. *Journal of Chemical Information and Modeling*, *53*(9), 1689–1699.

Yu, W., Sepehrnoori, K., & Patzek, T. W. (2016). Modeling Gas Adsorption in Marcellus Shale With Langmuir and BET Isotherms. *SPE Journal*, *21*(2), 589–600.

Zhang, W., Xu, J., & Jiang, R. (2017). Production forecast of fractured shale gas reservoir considering multi-scale gas flow. *Journal of Petroleum Exploration and Production Technology*, *7*(4), 1071–1083.

APPENDIX A

Reservoir Data

Parameter	Value	Units	Source
Methane velocity (ν)	0.322	ft/s	_
Methane viscosity (μ)	2×10^{-2}	cp	(Mengal, 2010)
Shale permeability (K)	500	nD	(Yu, 2015)
Gas density at reservoir conditions (ρ_g)	102.84	lb/ft^3	(Berawala, 2015)
Forchheimer parameter (β)	27.36	1/ft	calculated
α	0.8	_	_
Compressibility (c)	$6.30x10^{-5}$	1/psi	(Berawala, 2015)
Total compression (Ct)	10^{-6}	1/psi	(Yu,2015)
Knudsen number (K_n)	0.122	_	calculated
Shale density at reservoir pressure (ρ_R)	168.55	lb/ft3	(Berawala, 2015)
Maximum adsorption gas volume (v_m)	108.34	scf/ton	(Yu, 2015)
Saturation pressure (p_0)	21030.5	psi	(Wei Yu, 2014)
Initial reservoir pressure (p)	3100	psi	(Berawala, 2015)
Constant of net heat of adsorption (C)	36.88	_	_
Knudson diffusion coefficient (D_k)	$3.6x10^{-5}$	ft^2/s	calculated
Diffusion coefficient in the matrix (D_m)	$8.65x10^{-7}$	ft^2/s	calculated
Radius of sphere (r)	20	ft	(Berawala, 2015)
Reservoir porosity (Ø)	0.06	_	(Marthinus Cloete, 2010)
Reservoir temperature (T)	340	K	(Yu, 2015)
Langmuir pressure (P_L)	1240	psi	(Yu, 2015)
Maximum amount of adsorbed gas (V_L)	160.3	scf/ton	(Yu, 2015)
Dimensionless constrictivity factor (δ)	0.764	_	_

Tortuosity (τ)	2.532	_	_
Gas saturation (Sg)	1	_	_
Diameter of pore (d)	3	nm	_
Diameter of gas molecule (σ)	380	pm	_

Calculations

$$\delta = (1 - \frac{dgas}{dpore})^2$$

$$\delta = (1 - \frac{3.8\times10^{-10}}{3\times10^{-9}})$$

$$\delta = 0.764$$

$$\tau = \frac{1}{\emptyset^{1/3}\, Sg^{7/3}}$$

$$\tau = \frac{1}{(0.06)^{1/3}\,(1)^{7/3}}$$

$$\tau = 2.532$$

$$\lambda = \frac{k_B T}{\sqrt{2\pi\sigma^2 p}}$$

$$\lambda = \frac{1.3805\times10^{-23}\times340}{\sqrt{2\pi(3.8\times10^{-10})^2\times2\times10^7}}$$

$$\lambda = 3.658 \times 10^{-10}$$

$$K_n = \frac{\lambda}{d}$$

$$K_n = \frac{3.658\times10^{-10}}{3\times10^{-9}}$$

$$K_n = 0.122$$

$$D_k = \frac{2r}{3}\left(\frac{8RT}{\pi M}\right)^{0.5}$$

$$D_k = \frac{2(7.5\times10^{-9})}{3}\left(\frac{8\times8.314\times340}{\pi\times0.016}\right)^{0.5}$$

$$D_k = 3.35\times10^{-6}$$

$$D_m = \frac{\delta}{\tau}\ \emptyset\ D_k$$

$$D_m = \frac{1}{2.5}\ 0.06\ \times 3.35\times10^{-6}$$

$$D_m = 8.04\times10^{-8}\ m^2/s$$

APPENDIX B

MATLAB script file

Boundary conditions: @x = 0, P = Pi = 3100psi and @x = X, dp/dx = 0; where X represents the final or outer boundary co-ordinate.

```
m=0;
x=linspace(0,200,100);
t=linspace(0,6802,100);
u=pdepe(m,'pdex1pde','pdex1ic','pdex1bc',x,t);
surf(x,t,u)
xlabel('distance')
ylabel('time')
function [c,f,s]=pdex1pde(x,t,u,dudx)
c=-5.059*(10^-3);
f=dudx;
s=-9.53;
end
function u0=pdex1ic(x)
u0=3100;
end
function[pl,ql,pr,qr]=pdex1bc(xl,ul,xr,ur,t)
pl=u1-3100;
ql=0;
pr=0;
ql=1;
plot(x,u(end,:));
xlabel('distance');
ylabel('time');
end
```